



# Inorganic suspended matter as an indicator of terrestrial influence in Baltic Sea coastal areas — Algorithm development and validation, and ecological relevance

Susanne Kratzer<sup>a,\*</sup>, Dmytro Kyryliuk<sup>a</sup>, Carsten Brockmann<sup>b</sup>

<sup>a</sup> Department of Ecology, Environment and Plant Sciences, Stockholm University, 10691 Stockholm, Sweden

<sup>b</sup> Brockmann Consult GmbH, Chrysanderstr. 1, 21029 Hamburg, Germany

## ARTICLE INFO

Edited by Menghua Wang

### Keywords:

Inorganic suspended matter  
Remote sensing reflectance  
Particle scatter  
White scatterers  
Algorithm development  
Sentinel-3 Ocean and Land Colour Instrument (OLCI)  
C2RCC neural net  
SNAP  
Light limitation  
Baltic Sea

## ABSTRACT

Suspended particulate matter (SPM) consists both of an organic (OSPM) and an inorganic fraction (ISPM) and the latter can be used as an indicator for coastal influence in the Baltic Sea. The concentration of SPM can be derived from particle scatter if the specific scattering properties of the respective water body are known. In this paper we show that likewise, ISPM can be derived reliably from remotely sensed particle scatter. An empirical algorithm between particle scatter (AC9 data) and ISPM concentration (measured gravimetrically) was derived from in-water measurements. This regional algorithm was then applied to the *iop\_bpart* level 2 product (i.e. the particle scatter measured at 443 nm) derived from OLCI data on Sentinel-A (S3A) using the C2RCC neural network and validated against an independent data set. The standard error of the derived OLCI match-up data was 10%, and was thus within the goal of the mission requirements of Sentinel-3.

The generated S3 composite images from spring and autumn 2018 show that in the Baltic Sea most of the ISPM falls out rather close to the shore, whereas only a very small proportion of ISPM is carried further off-shore. This is also supported by in situ ISPM transects measured in the coastal zone.

The ISPM images clearly highlight the areas that are most strongly influenced by terrestrial matter. Differences between the NE Baltic and the SE Baltic proper can be explained by the difference in hydrology and coastal influence as well as bathymetry and wind-wave stirring. The method is of interest for coastal zone management and for assessing the effect of seasonal changes in terrestrial run-off and wind-driven resuspension of sediments. It can also be used to evaluate the effect of climate change which has led to an increase of extreme storm and flooding events that are usually accompanied by increased erosion and run-off from land. Last but not least, turbidity caused by particles influences the light conditions in inner coastal areas and bays, which has a profound effect on pelagic productivity, the maximum growth of macroalgae as well as fish behaviour.

## 1. Introduction

The colour of the sea has been widely used to evaluate water quality, e.g. using the Forel-Ule colour scale (Graham, 1966; Arnone et al., 2004) and since the 80s satellites have been used to derive water quality from space. The three main optical in-water components influencing the colour of the sea are: coloured dissolved organic matter (CDOM), SPM and phytoplankton pigments, often represented by the concentration of chlorophyll-a (Chl-a). In 1977, Morel and Prieur introduced an optical classification of natural waters: case 1 waters refers to waters where – besides water itself – phytoplankton and co-varying materials (i.e. detritus and CDOM) dominates the optical signal. In such waters, Chl-a can be retrieved from simple blue to green band ratios.

However, this relationship fails in optically-complex waters such as the Baltic Sea. In these so-called optical case 2 waters the optical signal is also influenced by CDOM and SPM. The early NASA SeaWiFS protocols (Mueller and Austin, 1995) distinguished between optical case 1 and case 2 as follows: case 1 waters are waters where CDOM absorption at 380 nm is  $< 0.1 \text{ m}^{-1}$  and the SPM concentration is below  $0.5 \text{ g m}^{-3}$ . In the Baltic Sea CDOM absorption at 440 nm ranges between 0.2 and  $13 \text{ m}^{-1}$  (Kratzer and Moore, 2018 and the literature cited therein) which means that all Baltic Sea waters are optical case 2 waters. SPM is moderately high in the Baltic Sea and ranges from about 0.2 to  $32 \text{ g}^{-3}$ . Kratzer and Tett (2009) showed that in the Baltic Sea the inorganic part of the suspended matter can be used as an indicator for coastal waters as the inorganic matter tends towards zero at about 10–15 km offshore.

\* Corresponding author.

E-mail address: [Susanne.Kratzer@su.se](mailto:Susanne.Kratzer@su.se) (S. Kratzer).

<https://doi.org/10.1016/j.rse.2019.111609>

Received 27 June 2019; Received in revised form 11 December 2019; Accepted 13 December 2019

0034-4257/ © 2019 The Authors. Published by Elsevier Inc. This is an open access article under the CC BY-NC-ND license (<http://creativecommons.org/licenses/by-nc-nd/4.0/>).

The trendlines for ISPM from summer showed that most of the inorganic fraction falls out steeply in the very inner coastal areas. This was confirmed in a recent study by Kari et al., 2018 using data from spring.

The attenuation of light and thus changes in the water-leaving reflection are caused by a combination of absorption (a) and scattering (b) of sun light by water itself and the optical components contained in the water. The main absorbing in-water components in coastal waters are CDOM as well as phytoplankton, which has two major absorption peaks in the blue and in the red (Kirk, 2011). The main scattering agent is inorganic suspended particulate matter (ISPM) which consist mostly of mineral particles such as sand, silt and clay. The particle scatter is determined by the particle type, size and the internal refractive index (Zaneveld et al., 1974; Mobley et al., 2002). CDOM consists of humic and fulvic acids and absorbs light in the blue-green region of the spectrum (Kirk, 1976, 2011) and its absorption spectrum decreases logarithmically from blue towards red. Non-algal organic suspended particulate matter (OSPM) consists of degraded plant matter and has a similar absorption spectrum to CDOM but a different logarithmic slope factor. A lower reflectance in the blue-green is thus mostly caused by high concentrations of CDOM and/or OSPM, and with increasing absorption in the blue the reflectance peak is progressively moved towards the red part of the spectrum. ISPM, however, has a large refractive index and a relatively high backscatter,  $b_b$  (Stramski et al., 2004; Boss et al., 2004), and therefore produces reflectance spectra several orders greater in magnitude than waters rich in CDOM, or only containing phytoplankton (Dierssen et al., 2006). Thus, ISPM can be traced by satellite due to its strong scattering properties, making satellite images look brighter, even when there is a high CDOM background absorption. The backscatter ratio  $\tilde{b} = b_b/b$  in coastal turbid waters is commonly assumed to be 0.0182, the value observed by Petzold (1972). Kratzer and Moore (2018) found that the mean backscatter ratio for the Baltic Sea is 0.0170, and thus about 6.6% lower than the value observed by Petzold.

In recent years, ESA launched the Copernicus mission consisting of a system of so-called Sentinel satellites to monitor the Earth's surface and environmental changes continuously until about 2030. The Sentinel-3 series of satellites (S3A-S3D) are dedicated to monitoring the world's oceans and seas. The first two satellites, S3A and S3B were launched in early 2016 and early 2018, respectively. S3 houses the Ocean and Land Colour Scanner (OLCI) which is based on the experience from ESA's previous mission, ENVISAT, with improved capabilities. ENVISAT was the platform for the Medium Resolution Imaging Spectrometer (MERIS), which has been ESA's flagship for coastal remote sensing due to its improved spatial and spectral resolution compared to previous ocean colour sensors (Doerffer et al., 1999). Due to the ENVISAT mission, coastal and lake remote sensing research has been vastly accelerated (Kratzer et al., 2008; Odermatt et al., 2012; Blondeau-Patissier et al., 2014; Harvey et al., 2015; Vaičiūtė et al., 2015; Beltrán-Abaunza et al., 2016; Alikas and Kratzer, 2017).

The retrieval of water constituents from optically-complex waters is typically achieved by inversion of the water-leaving reflectance spectrum (Schiller and Doerffer, 1999; Doerffer and Schiller, 2007; Schroeder et al., 2007a, 2007b) which has been measured from space (top-of atmosphere radiance) and subsequently been corrected for atmospheric effects. The Case-2 Regional (C2R) processor is one of the most widely used coastal processors and was originally developed by Doerffer and Schiller (2007). It uses a large database of radiative transfer simulations inverted by neural networks (NN) as underlying technology. Along with other coastal processors it has been tested intensively in the Baltic Sea (Kratzer and Vinterhav, 2010; Attila et al., 2013; Beltrán-Abaunza et al., 2016; Vaičiūtė et al., 2015). Through the recent ESA CoastColour (CC) project major improvements were introduced to the initial C2R processor. It has been further trained to cover extreme ranges of scattering and absorption and is capable of processing data from ESA's OLCI, MSI, MERIS as well as NASA's VIIRS,

MODIS and Landsat-8 instruments. The current version of the processor is called Case-2 Regional CoastColour (C2RCC). This processor (Brockmann et al., 2016) has been validated in a large number of coastal study sites during the ESA CoastColour project (<http://www.coastcolour.org>) and is available through ESA's Sentinel toolbox SNAP (ESA, n.d.). C2RCC is currently also used in the Sentinel-3 OLCI ground segment processor of ESA/EUMETSAT for the generation of water products for optically-complex waters.

Historically, the main biogeochemical products derived from ocean colour data were SPM, Chl-a and CDOM. In the C2RCC these products are then derived from the inherent optical properties (IOPs) of each of the optical components, i.e. the absorption and scattering properties using a neural network (NN) approach which applies an iterative fitting procedure. Absorption and scattering, in return can be derived from reflectance data as the marine reflectance is a direct function of the IOPs. The C2RCC processor provides absorption and scattering at 443 nm from which the main optical components can be derived if the regional specific IOPs are known. Examples of specific IOPs are the Chl-a-specific absorption as well as the SPM-specific scatter or backscatter (Kratzer, 2000; Doerffer, 2002).

Another water-quality parameter that can be derived from remote sensing data is turbidity. It is strongly related to the SPM concentration (Nechad et al., 2010; Dogliotti et al., 2015; Kari et al., 2017). In recent years, turbidity has been included in the Swedish coastal monitoring program as an additional water quality parameter. Turbidity measured in situ is an efficient and cost-effective way to measure the influence of suspended particles in the coastal zone while measuring SPM gravimetrically is rather time consuming process. The underlying physical process for measuring suspended particle via turbidity is that particles causes scatter of light which is proportional to the concentration of SPM in natural waters. Turbidity (ISO 7027) is thus a measure of the reduction of light transparency in the near-infrared (860 nm) caused by the presence of particles. Kyrliuk and Kratzer (2019) tested a new turbidity algorithm on Sentinel-3 data that is based on the relationship between turbidity and particle scatter. This regional algorithm had relatively low uncertainties with a mean normalized bias (MNB) of 2.8%, a root mean square error (RMSE) of 35% and a mean absolute percent difference (MAPD) of 34% when tested against an independent data set.

As most of the scatter, and thus the turbidity, is caused by inorganic particles, we aim here to evaluate the empirical relationship between (A) ISPM and turbidity for Baltic Sea waters and to compare this to the relationship between (B) organic SPM (OSPM) and turbidity in order to assess which is the better predictor, i.e. to assess if it is mostly the inorganic or organic fraction of the suspended matter that causes particle scatter, and thus turbidity.

Further, we aim to retrieve ISPM from S3 OLCI data over the Baltic Sea using the C2RCC in order to highlight those areas that are most influenced by land and wind-driven resuspension in shallow areas (using ISPM as indicator). We thus aim to derive the empirical relationship between C) ISPM and particle scatter at 440 nm,  $b_{440}$ , measured in situ in the Baltic Sea (with an AC9), and subsequently to apply this empirical relationship to OLCI level 2 data in order to derive ISPM and finally, to validate the derived product against an independent data set measured at the time of satellite overpass (match-up data). The analysis is done via empirical regression algorithms applied to in-water measurements, and these empirical relationship can then be applied to the *iop\_bp* product of the C2RCC neural network to derive ISPM from remote sensing reflectance. We also evaluate the relationship D) between organic SPM (OSPM) and particle scatter in order to investigate in as how much organic particulates contribute to particle scatter.

Besides this, the seasonal distribution of ISPM in coastal areas will be evaluated using ISPM data measured in situ (spring vs. summer distribution) and plotted against horizontal distance from station H6 in the inner Himmerfjärden bay. We also evaluate the changes in

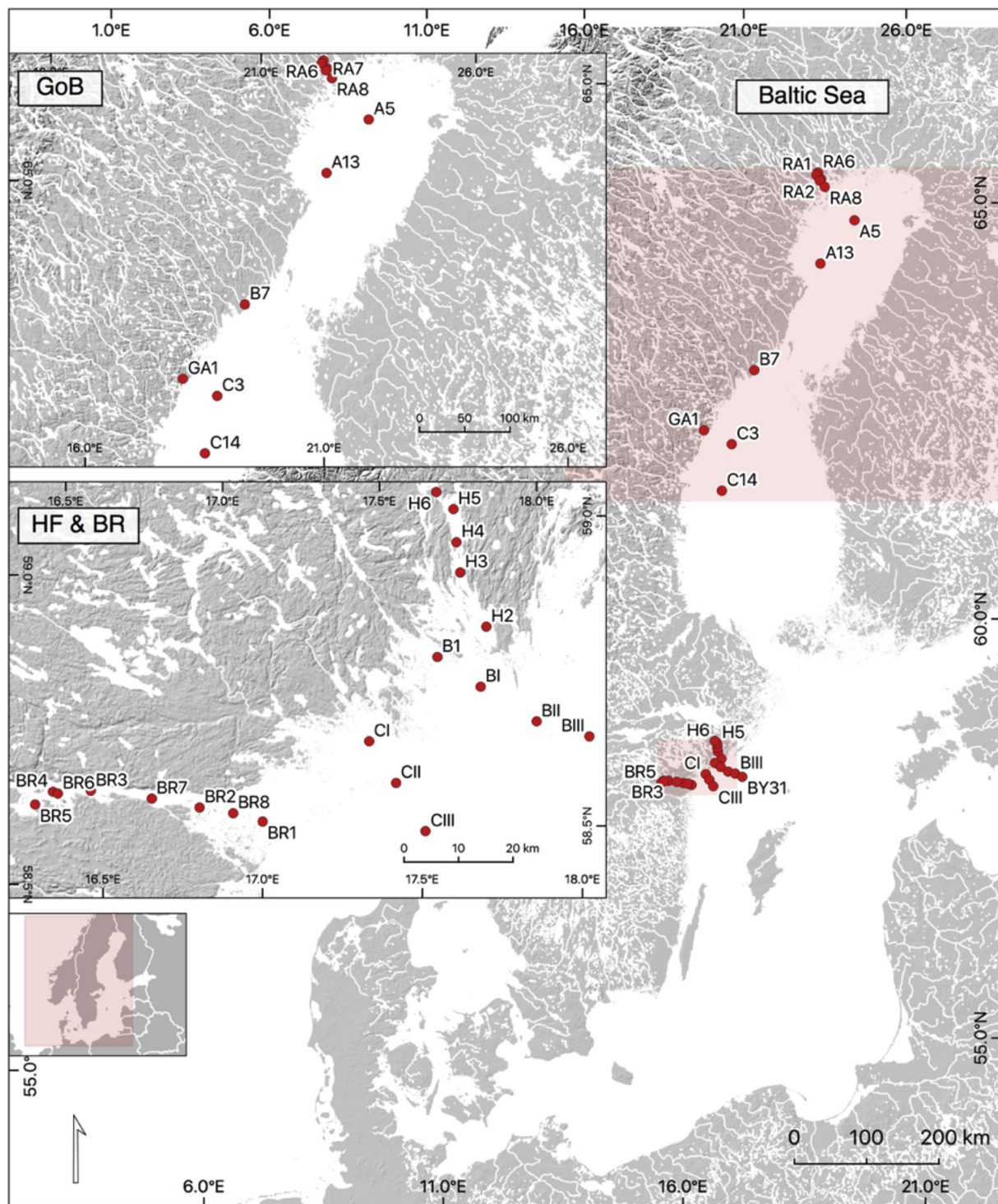


Fig. 1. Overview map of the nominal sampling stations of the dedicated bio-optical research campaigns in the Swedish coastal areas — Himmerfjärden (HF) and Bråviken (BR) and in the Gulf of Bothnia (GoB) used in the development and validation of Inorganic Suspended Particulate Matter algorithm. Coastline — Copernicus EU-DEM v1.1 (<https://land.copernicus.eu/imagery-in-situ/eu-dem/eu-dem-v1.1/view>). Lakes — Vogt, J.V. et al. (2007): A pan-European River and Catchment Database. European Commission — JRC, Luxembourg, (EUR 22920 EN) 120.

reflectance along an off-shore to near-shore gradient in Himmerfjärden and Bråviken bays as well as in the Bothnian Bay and investigate the influence of CDOM and SPM on the water-leaving reflectance. Furthermore, binned S3 OLCI ISPM L3 data (i.e. space and time averaged) from April 2018 will be used to map coastal run-off over the Baltic Sea basin and the difference in a range of coastal areas will be discussed. Additionally, a time-series of monthly composites

(April–September) of L3 data will be generated to show the monthly distribution of ISPM in the Baltic proper in the key productive seasons. The resulting images will be discussed using data from the literature. Last but not least, the ecological effects of coastal ISPM distribution will be discussed using examples from the literature.

## 2. Materials and methods

### 2.1. Area of investigation

The area of investigation is the north-western (NW) Baltic Sea and the western Gulf of Bothnia (Fig. 1). The empirical data for algorithm development was gathered during dedicated bio-optical research cruises in the NW Baltic proper during 2000–2014 (Kratzer et al., 2003; Kratzer and Tett, 2009; Kratzer and Vinterhav, 2010; Beltrán-Abaunza et al., 2016; Kari et al., 2017; Kari et al., 2018; Harvey et al., 2019). The optical in situ data was used to map the distribution of ISPM in the coastal zone measured in situ, and to develop empirical algorithms between A) ISPM and turbidity and B) OSPM and turbidity. For algorithm development, all data was ln-transformed as this led to a more even distribution of the residuals.

Additional dedicated optical cruises were performed during 2016–2018 in order to establish the relationship between ISPM and particle scatter,  $b_{440}$ . The aim was to cover areas with a relatively large range of SPM. Previous work with MERIS data over the NW Baltic Sea had shown that there is a relatively large range of SPM in Bråviken bay, situated south west of Askö (Vinterhav, 2008; Kyryliuk, 2014). Thus, during 2018, two transects with optical measurements were performed through Bråviken bay, BR1-BR4 and BR5-BR8 (Fig. 1). Furthermore, 3 optical cruises (lasting 4 days each) were performed on R.V. KBV181 across the Gulf of Bothnia, GoB (Fig. 1) in May (week 20), June (week 24) and July (week 28) 2018. These campaigns included a coastal station (B7) close to the mouth of the Öre Estuary (near Umeå), as well as at the Swedish High coast (GA1) and at coastal sites in the Råneå estuary (STNS RA1, RA2, RA6, RA8) in the NW Bothnian Bay as well as open sea stations in both the Bothnian Sea (C3, C14) and the Bothnian Bay (A5, A13). The coastal waters in the GoB were characterized by very strong coastal influence both after the ice thawing in spring and even during summer. This data set was then combined with an additional optical data set from 2012 from the Himmerfjärden area in order to derive a new regional ISPM- $b_{440}$  algorithm for S3 OLCI data ( $n = 46$ ). A separate subset of the 2016–2018 data was used to validate the satellite-derived ISPM data ( $n = 22$ ).

### 2.2. Optical in situ measurements

The optical measurements performed by the Marine Remote Sensing Group at Stockholm University over the last 2 decades were both aimed at validating satellite data (SeaWiFS, MERIS and OLCI) as well as creating an optical data base for regional algorithm development. In order to sample optical data that is representative for Baltic Sea waters, the measurements were usually performed along transects (30–60 km), following clear nearshore to off-shore gradients (Kratzer and Tett, 2009), and in more recent years also across different Baltic Sea basins (Harvey et al., 2015; Harvey et al., 2019).

#### 2.2.1. Deriving particle scatter

An AC9+ system (WetLabs, Philomath) fitted with a CTD (SAIV-AS, Norway) was used to measure absorption ( $a$ ) and beam attenuation ( $c$ ) in situ. The AC9 data was transferred from binary to engineering units using a custom Excel AC9 processor (Kratzer and Moore, 2018). This AC9 processor, developed by Bio-Optika (UK), applies the WetLabs calibration file (device file) and corrects the data for salinity and temperature measured by the CTD, and also for scatter from water,  $b_w$ . A total number of 76 AC9 profiles were measured during 2012, 2017 and 2018. The particle scatter at 440 nm,  $b_{440}$ , was derived from AC9 data by subtracting the total absorption measured by the AC9 from the beam attenuation each at 440 nm:  $b_{440} = c_{440} - a_{440}$ .

#### 2.2.2. Deriving water-leaving reflectance using a TACCS radiometer (Satlantic)

A TACCS (Tethered Attenuation Coefficient Chain-Sensor; Satlantic

Inc., Canada) was used for measuring upwelling radiance and downwelling irradiance, and to derive water-leaving reflectance. The TACCS is a radiometer system mounted on a floating buoy. It measures upwelling radiance,  $L_u(\lambda)$ , at 7 channels (412, 443, 490, 510, 560, 620 and 665 nm) at 50 cm below the sea surface.

The TACCS system also measures downwelling irradiance ( $E_d$ ) above the sea surface at 443, 490 and 670 nm, and has a chain of downwelling irradiance sensors  $E_d(490\text{ nm})$  at nominal depths of 2, 4, 6, and 8 m to derive  $K_d(490)$ . All TACCS sensors have a 10 nm bandwidth. TACCS measurements were logged over 2 min (at an acquisition rate of 1 Hz), approximately 20 m away from the ship in order to avoid ship shading. The water-leaving reflectance was derived from the TACCS data using a dedicated processor (Kratzer et al., 2008; Zibordi et al., 2012). For estimating upwelling radiance just below the surface, spectral  $K_d$  was derived from both spectral absorption and scatter measured with the AC9 according to Kirk (2011) and Kratzer et al. (2008). Subsequently, spectral  $K_d$  was used as an input into the TACCS processor in order to propagate the spectral upwelling radiance from 50 cm to just below the sea surface. The upwelling radiance above the sea surface was then derived by multiplying the radiance values with a factor of 0.54. Finally, the water-leaving reflectance,  $\rho$  (rhov) was estimated from the ratio of upwelling radiance and downwelling irradiance, multiplied by the factor of PI (3.14159). Note that the processor also includes a correction for instrument self-shading.

#### 2.2.3. Measuring inorganic and organic particles

Water samples were collected at about 15–20 cm below the sea surface at each optical station, using a dedicated, durable sampling bucket. The samples were treated according to the optical protocols detailed in Kratzer and Tett (2009) using the gravimetric method introduced by Strickland and Parsons (1972) and further developed in the MERIS protocols (Doerffer, 2002). The samples were filtered through pre-weighed and pre-combusted GF/F filters (with a nominal pore size of 0.7  $\mu\text{m}$ ). The filters had also been cleaned with ultra-pure water prior combustion. Each water bottle was gently mixed before filtration. For deriving suspended particulate matter, about 1–2 l of sea waters were filtered through 47 mm GF/F filters (triplicates for each station). The filters were rinsed with 100 ml ultrapure water (UPW) in order to wash out salt residuals. The filters were then dried over night at 60 °C and kept in a desiccator until weighing. The (total) suspended particulate matter was calculated as the difference between the dry and the tare weight. Then the filters were combusted at 480 °C and weighed again, to derive the weight of the inorganic particles (combusted weight minus tare weight). The organic fraction was then derived from the difference between the total and the inorganic fraction. In order to correct for handling errors 10 blank filters were processed in the same way by filtering 1 l of ultrapure water and the average blank values were used to correct the sample filters.

The triplicate results for each station were quality checked as it is easy to lose a part of the filter in the handling process. If a replicate deviated > 20% from the other samples it was not used for deriving the average value for the respective station. The weighing was done with a Satorius MP3 microbalance. The standard error of the method is 10% (Kratzer, 2000).

#### 2.2.4. Turbidity measurements

The turbidity was measured using a portable bench turbidity meter (Hach Lange 2100Qis) calibrated against standard Formazin solutions provided by the manufacturer (10, 20, 100, 800 NTU). The turbidity is subsequently given in Formazin Nephelometric Unit (FNU). The samples were gently mixed before each measurement and the sample was measured only after 10 s to allow air bubbles to escape. During each campaign the turbidity meter was calibrated against the standard solutions provided by the manufacturer. On each sampling day this calibration was checked against the 10 NTU calibration solution. If this calibration check did not give a pass the full calibration was repeated.

Each sample was measured in triplicates (Kari et al., 2017) and corrected for the turbidity of ultrapure water (also measured in triplicates).

### 2.2.5. Algorithm development based on in situ data

The relationships between A) ISPM and turbidity and between B) OSPM and turbidity were derived empirically by least-square linear regression analysis of the LN-transformed data using data from the NW Baltic Sea (including Bråviken bay) from 2016 to 2018. All least-square regressions were performed in Systat 13, and can be written as:

$$\ln(\text{ISPM}) = 1.42 \pm 0.1 * \ln(\text{turbidity}) - 0.82 \pm 0.08 \quad (\text{A})$$

The coefficient of determination was:  $R^2 = 0.83$  ( $n = 44$ ) and the slope coefficient as well as the intercept were significant with  $p = 0.000$ , each.

$$\ln(\text{OSPM}) = 0.462 \pm 0.076 * \ln(\text{turbidity}) - 0.233 \pm 0.059 \quad (\text{B})$$

The coefficient of determination was:  $R^2 = 0.46$  ( $n = 44$ ) and the slope coefficient as well as the intercept were significant with  $p = 0.000$ , each. Note that the regression plots for Eqs. (A) and (B) are shown in the results section (Fig. 4a and b). Next, a multiple regression analysis was performed in order to see if turbidity can be best predicted from ISPM and OSPM concentrations combined (as suggested by the regression analyses above).  $\ln(\text{turbidity})$  was chosen as the dependent variable as it depends on the concentration of particles by definition. The results of the multiple regression analysis can be written as:

$$\ln(\text{turb}) = 0.55 \pm 0.06 * \ln(\text{ISPM}) - 0.11 \pm 0.013 * \ln(\text{OSPM}) + 0.48 \pm 0.06 \quad (\text{AB})$$

The  $p$  values for the ISPM coefficient and for the intercept each were  $p = 0.000$ , which means they are significant. However, the  $p$  value for the OSPM coefficient was  $p = 0.39$ , indicating that OSPM is not a significant or a meaningful addition to the regression model.

When testing the ISPM-turbidity algorithm (Eq. (A)) against an independent data set from the NW Baltic Sea during 2010–2011 (monitoring cruises described in Harvey et al., 2019) the correlation coefficient was  $r = 0.99$ ;  $n = 36$ . This means that ISPM can be derived reliably from turbidity in Baltic Sea waters.

The data set measured during 2016–2018 in Himmerfjärden bay, Bråviken and the Gulf of Bothnia (GoB) was then combined with an additional data set from 2012 from the Himmerfjärden area in order to derive a new ISPM algorithm for S3 based on the relationship between ISPM and  $\text{bpart}_{440}$ . As there was no ISPM data available from the GoB, ISPM was estimated here from bench turbidity using Eq. (A), allowing to extend the range of ISPM concentrations from a minimum value of 0 to a maximum of  $9.73 \text{ g}^{-3}$  (corresponding to a measured turbidity of 8.9 FNU). Then, these synthesized ISPM data from the GoB along with the measured ISPM data from Bråviken and the Himmerfjärden area were regressed against  $\text{bpart}_{440}$  measured in situ by the AC9. The derived algorithm can be written as:

$$\ln(\text{ISPM}) = 1.23 \pm 0.14 * \ln(\text{bpart}_{440}) - 0.59 \pm 0.1 \quad (\text{C})$$

The coefficient of determination was:  $R^2 = 0.67$  ( $n = 46$ ) and the slope coefficient as well as the intercept were significant with  $p = 0.000$ , each. The regression plot is shown in Fig. 5a) in the results section. Additionally, the regression between  $\ln(\text{OSPM})$  and  $\ln(\text{bpart}_{440})$  was evaluated on the in situ data set from 2016 to 2018. The results showed only a modest dependency of  $\ln(\text{OSPM})$  and  $\ln(\text{bpart}_{440})$ , see also Fig. 5b:

$$\ln(\text{OSPM}) = 0.25 \pm 0.084 * \ln(\text{bpart}_{440}) \quad (\text{D})$$

The coefficient of determination was:  $R^2 = 0.19$  ( $n = 46$ ) and the coefficient for the intercept was not significant, and the intercept was therefore omitted. Next, a multiple regression analysis was performed in order to see if  $\text{bpart}_{440}$  can be predicted more reliably from a combination of ISPM and OSPM concentrations (as suggested by the

regression analyses above).  $\ln(\text{bpart}_{440})$  was chosen as the dependent variable as particle scatter is directly related to the concentration of particles in the water. The results of the multiple regression analysis can be written as:

$$\ln(\text{bpart}_{440}) = 0.626 \pm 0.084 * \ln(\text{ISPM}) - 0.327 \pm 0.224 * \ln(\text{OSPM}) + 0.348 \pm 0.077 \quad (\text{CD})$$

The coefficient of determination was:  $R^2 = 0.69$  ( $n = 46$ ), which means not significantly higher than for the single regression between  $\ln(\text{ISPM})$  and  $\text{bpart}_{440}$ . The  $p$  values for the ISPM coefficient and for the intercept each were  $p = 0.000$ , which means they are significant. However, the  $p$  values for the OSPM coefficient was  $p = 0.152$ , indicating that OSPM is neither here a significant or a meaningful addition to the regression model. Thus, the empirical algorithm between ISPM and  $\text{bpart}_{440}$  (Eq. C) based on optical in-water measurements was applied to the OLCI  $\text{iop\_bpart}$  product in order to derive ISPM (see Section 2.3.3 below).

## 2.3. Sentinel-3A data processing and algorithm validation

### 2.3.1. Data download

The data used for application and validation of the ISPM algorithm Level-1b (L1b) data from Sentinel-3A were downloaded from the EUMETSAT Copernicus Online Data Access (CODA-REProcessed; <https://codarep.eumetsat.int>) for scenes between 2016 and 2017 and from the on-going CODA portal (<https://codarep.eumetsat.int>) for the scenes in 2018. In total, 15 L1b products were downloaded covering the dates of dedicated sampling campaigns in the NW Baltic Sea. By using CODA-REP for historic data and CODA for recent data, we assure that all data were processed with a consistent processing baseline.

### 2.3.2. Atmospheric correction

The L1b data were atmospherically corrected applying the C2RCC v. 1.0 OLCI processor (version 1 nets — 2016) without vicarious calibration in the ESA SNAP toolbox v.6.0. Note that standard atmospheric correction procedures often produce negative reflectances in the blue for the highly absorbing water of the Baltic Sea. The water-leaving reflectance in the blue is so small, that a slight overestimation of the atmospheric path radiances immediately leads to a negative reflectance after atmospheric correction, and hence invalid retrievals which cannot be further evaluated.

### 2.3.3. Retrieval of IOPs and ISPM

IOPs were also retrieved with the C2RCC SNAP processor. As mentioned before the processor uses a neural net for inversion of the radiative transfer function. The net has been trained with the directional water-leaving reflectance of all OLCI bands (except the atmospheric absorption bands 13, 14, 15, 19 and 20) as input, and 5 IOP components as output. The 5 components are the chlorophyll-a absorption, scattering by particles, scattering by a white scatterer (i.e. an in-water scatterer with a spectral slope exponent of 0), CDOM absorption and detritus absorption. The conversion of the IOPs is based on the specific inherent optical properties, and thus is region specific. C2RCC provides defaults which were derived from analysis of the global NASA Bio-Optical Marine Algorithm Dataset (NOMAD, n.d.; Werdell and Bailey, 2005). In SNAP a number of processing parameters can be freely defined via a user interface; if the parameters are not changed the default values are used. In order to correct the water absorption for salinity and temperature effects the processor requires appropriate parameterisation of these two parameters. Therefore, salinity and temperature were modified to local, user-defined average values measured during the validation campaigns and climatology data was automatically imported from L1b data (by ticking the option ‘use of ECMWF aux data of the source product’).

For regional SPM retrieval, the factor for the parameter  $\text{iop\_bpart}$

(particle scatter) was set to 0.984, i.e. the inverse of the Baltic Sea-specific scatter described in Kratzer and Moore (2018), and  $b_{wit}$  was set to a value of 1.72 as this has shown to deliver reliable results for the Baltic Sea (Kyrlyuk and Kratzer, 2019). The default value for  $b_{wit}$  is 3.1. It was developed as a flag for strong white scatterers, such as coccoliths, white caps and air bubbles. Coccoliths, however, do not occur in the Baltic Sea, and 3.1 is thus too high for the Baltic Sea.

Furthermore, the empirical regression in-water algorithm between ISPM and particle scatter, was applied to the scattering coefficient at 443 nm, i.e. the  $iop_{bpart}$  product derived from OLCI C2RCC-SNAP Level 2 data in order to generate ISPM concentrations. It was assumed that the 3 nm shift compared to  $b_{440}$  derived from the AC9 did not make a significant difference in the results.

#### 2.3.4. Data quality flagging

A set of quality flags generated by C2RCC-SNAP was applied in order to remove image pixels where the inversion of the satellite signal failed, from further processing. A combined valid-pixel expression was constructed to

- check if the signal measured by the satellite is contained in the training database of the AC neural net. This condition is checked by C2RCC using an auto-associated neural net and the result is coded in the Rhov\_OOS flag;
- check on cloud risk which is (often) indicated by a high downwelling transmission, derived by C2RCC and coded in a dedicated flag (Cloud\_risk);
- check on optical closure: the IOPs retrieved by C2RCC from rho\_w are fed into a neural net which approximated a radiative transfer model and estimate the water leaving spectrum (rho\_w\_fw). In case of optical closure, i.e.  $\rho_{w\_fw} = \rho_w$ , the IOPs are confirmed a valid solution of the radiative transfer problem. If not, and depending on the magnitude of the mismatch, a flag is raised by C2RCC (Rhov\_OOS).

The Level-2 (L2) products generated by the C2RCC-SNAP processor were then extracted using the pin-pixel extraction tool of SNAP and subsequently compared to the values measured in situ. A  $1 \times 1$  pixel window was chosen as match-up window instead of the  $3 \times 3$  macropixel more commonly applied for match-up analysis in coastal waters (Kratzer and Vinterhav, 2010; Beltrán-Abaunza et al., 2016). The  $1 \times 1$  pixel window was chosen in order to reduce the already existing spatial discrepancy and related uncertainties between in situ and satellite data caused by the time differences between in situ measurement and satellite overpass and thus the movement of water due to currents. A pre-evaluation of the match-up data (using the flag expression cloud\_risk) had shown that individual pixels provided a lower number of match-ups ( $n = 22$  vs.  $n = 26$ ) compared to  $3 \times 3$  macropixels, while, however, the correlation coefficient was substantially improve and at the same time the uncertainties were substantially reduced.

#### 2.3.5. ISPM validation

After pixel extraction of the match-up data, the ISPM product was compared to an independent data set of ISPM measured in situ (match-up analysis). The correlation between predicted and measured data was evaluated statistically using Spearman correlation. Then uncertainties were estimated using the Mean Normalized Bias (MNB) as a measure of systematic off-set, the Root Mean Square Error (RMSE) as a measure of the relative error, and the Mean Absolute Percentage Difference (MAPD); note that all error metrics are given in % (Cristina et al., 2009; Kratzer and Vinterhav, 2010; Beltrán-Abaunza et al., 2016; Kyrlyuk and Kratzer, 2019):

$$(MNB), (\%) = \frac{1}{n} \sum_{i=1}^n \left( \frac{OLCI_i - in situ_i}{in situ_i} \right) \times 100$$

$$(RMSE), (\%) = \sqrt{\frac{1}{n} \sum_{i=1}^n \left( \frac{OLCI_i - in situ_i}{in situ_i} \right)^2} \times 100$$

$$(MAPD), (\%) = \left( \exp \left( \text{mean} \left| \ln \left( \frac{OLCI_i - in situ_i}{in situ_i} \right) \right| \right) - 1 \right) \times 100$$

The statistical analysis was performed both in Excel and Systat 13 and the results were plotted in Excel.

#### 2.3.6. Deriving an ISPM-composite image for April 2018

In order to show the effect of coastal influence we chose April 2018 for L3 binning of available ISPM data as April is the time of year when there is a lot of coastal influence after the ice thawing in spring. Furthermore, we evaluated the data from the Himmerfjärden Eutrophication Study (<http://www2.ecology.su.se/dbhfj/index.htm>) which indicated that the spring bloom and usually happens around mid-April in the Baltic proper. All available scenes from April 2018 thus were downloaded and processed in the same way as outlined above and the Level-3 (L3) OLCI product for ISPM was generated using the Level-3 binning procedure based on the NASA SeaWiFS binning algorithm (Campbell et al., 1996), performing spatial and temporal aggregation of pixel values into statistically averaged (bins). This L3 product thus shows the average monthly concentration and distribution of inorganic suspended matter for April 2018. The same approach was used to further generate a monthly time-series (April–September 2018) to highlight the seasonal distribution of ISPM in the Baltic proper.

### 3. Results

#### 3.1. Distribution of inorganic matter in near-coastal areas and further off-shore

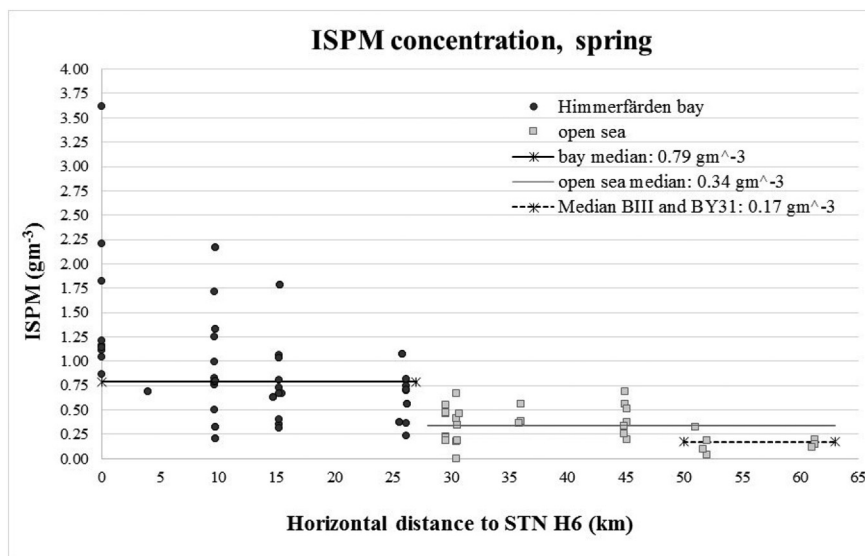
The coastal data set from Himmerfjärden (2000–2018) was used to investigate the seasonal influence on the distribution of ISPM along 2 horizontal transects I) through Himmerfjärden and II) from B1 out to Landsort Deep (BY31), following the method established by Kratzer and Tett (2009). Fig. 2 shows differences in the ISPM concentrations from the inner bay (STN 6) to BY31 during (a) spring (March–May) and (b) summer (June–August) as derived from in-water measurements. During spring, the median ISPM concentration inside the bay ( $0.79 \text{ g}^{-3}$ ) is only slightly higher than in summer ( $0.77 \text{ g}^{-3}$ ), however, the standard deviation is much higher in spring ( $\pm 0.63 \text{ g}^{-3}$ ) than during summer ( $\pm 0.37 \text{ g}^{-3}$ ), indicating a much higher variability. The higher ISPM concentration in spring than in summer (Fig. 2a vs. b) can partially be explained by increased run-off after the ice thawing period. In spring, twice as much ISPM reaches the open sea with a median value of  $0.34 \text{ g}^{-3}$  ( $\pm 0.18 \text{ g}^{-3}$ ) than during summer with a median value of  $0.17 \text{ g}^{-3}$  ( $\pm 0.18 \text{ g}^{-3}$ ), the variance of both data sets was 3%.

The remote sensing reflectance (Fig. 3) in the coastal zone changes with changing ISPM and CDOM concentrations in the different coastal areas (Bråviken, Himmerfjärden and Råneå area).

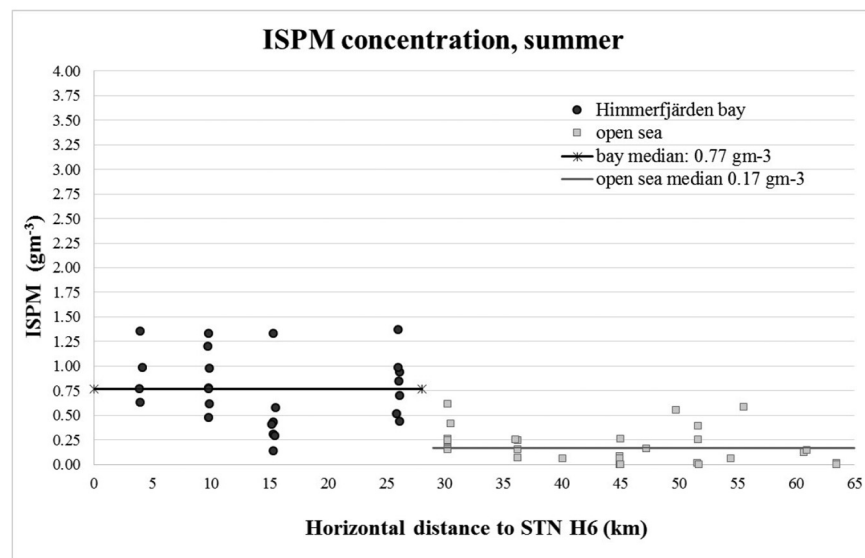
#### 3.2. Results of the algorithm development

As already mentioned in the methods section the relationship between  $\ln$  (turbidity) and  $\ln$ (ISPM) was significant, and the correlation coefficient between the variables was very strong (Fowler et al., 1998) with  $R = 0.91$  (note the corresponding regression model is shown in Fig. 4). The relationship between  $\ln$ (ISPM) and  $\ln$ (turbidity), however, only showed a modest correlation with  $R = 0.68$  (Fowler et al., 1998) between the two variables (the regression model is shown in Fig. 4b).

The relationship between  $\ln$ (ISPM) and  $\ln$  ( $b_{part440}$ ) also showed a strong dependency, with  $R = 0.82$ , the regression between the two variables is shown (Fig. 5a). The relationship between  $\ln$ (ISPM) and  $\ln$  ( $b_{part440}$ ) only showed a modest dependency between the two



(a)



(b)

**Fig. 2.** Distribution of inorganic suspended particulate matter (ISPM) in Himmerfjärden bay and the open Baltic Sea during spring (a) and summer (b). The concentrations are shown here in relation to the horizontal distance (in km) from Station H6 situated in the inner bay, reaching out to Landort deep at about 65 km away from H6. The graphs show that in spring, ISPM is much higher inside the bay (black dots) than off-shore (grey dots). The concentration drops rather shortly outside the bay as the larger particles fall out close to the coast and only small inorganic solids (i.e. silt particles) are carried further offshore. In general, the concentration of particles at Landort deep and surrounding waters tends towards a median of about  $0.17 \text{ g}^{-3}$ .

variables ( $R = 45$ ). The regression shown in Fig. 5b) proofed to be significant (see Materials and methods section). However, the multiple regression analysis between  $\text{bpart}_{440}$  and both  $\ln(\text{ISPM})$  and  $\ln(\text{OSPM})$  showed that OSPM is not a meaningful contribution to regression model.

### 3.3. Algorithm validation

The dedicated match-up analysis showed that there was a very strong correlation with  $R = 0.95$  (Fowler et al., 1998) between satellite-derived and in situ ISPM data (Fig. 6) and the correlation was significant ( $p < 0.05$ ,  $n = 22$ ). The Mean Normalized Bias was ( $-24\%$ ), and the Root Mean Square Error was  $52\%$  and the Absolute Percentage Difference was  $89\%$ . The values above  $1.0 \text{ g}^{-3}$  showed on average a slightly stronger underestimation of about  $-30\%$ . These higher values were all measured in the inner bay (at stations H3, H4 and H6). The standard error ( $\sigma$ ) for the in situ data was  $12\%$  and thus comparable to total SPM (Kratzer, 2000). For the OLCI-predicted data it was  $9\%$  which is within the  $10\%$  goal of the S3 Mission Requirements Document (ESA, 2007).

### 3.4. Applications of ISPM algorithm

Fig. 7 shows a) the monthly composite of total SPM derived from OLCI data and b) shows the monthly composite of ISPM generated by applying the in-water algorithm (Eq. C) to OLCI data. The composite image of total SPM (Fig. 7a) shows that the highest SPM values are found in near-coastal areas, and moderate concentrations of (total) SPM are even found off-shore. The ISPM image, however, shows a very different distribution pattern (Fig. 7b). High ISPM values are also mostly confined to near-coastal and shallow areas (different grades of red and pink) but ISPM converges towards very low values in the open southern Baltic proper and the northern Gulf of Bothnia (around  $0.03 \text{ g}^{-3}$ ) and around  $0.2 \text{ g}^{-3}$  in the off-shore waters close to Himmerfjärden (Fig. 8) which corresponds approximately to the median open sea values measured in situ during spring time (Fig. 2).

## 4. Discussion

The main aim of this paper was to describe the relationship between inorganic particles and scatter based on optical in situ measurements

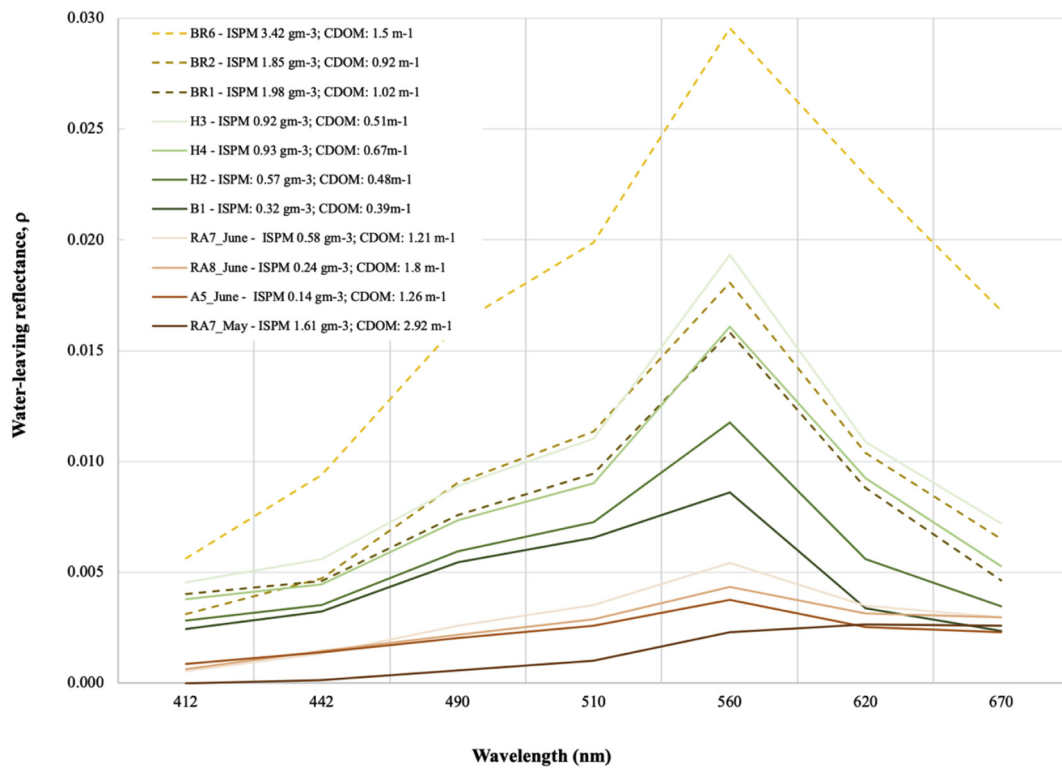


**Fig. 3.** In situ water-leaving reflectance measured with the TACCS radiometer in Himmerfjärden bay (green spectra in the middle; B1 & H2–H4), Bråviken bay (upper, brown-yellow spectra, dashed; BR1–BR8) and in a coastal gradient in the Råneå area in the Bothnian Sea (brown solid spectra at the lower end; A5 & RA7–RA8). ISPM generally increases the reflectance especially in the green (560 nm), while CDOM, phytoplankton pigments and organic SPM reduce the reflectance. At very high CDOM absorption the maximum reflectance is shifted towards the red end of the spectrum (RA7). Note CDOM was measured in terms of absorption at 440 nm, commonly referred to as  $g_{440}$  (unit:  $m^{-1}$ ); ISPM was measured in  $gm^{-3}$ . (For interpretation of the references to color in this figure legend, the reader is referred to the web version of this article.)

and then to apply this empirical relationship to OLCI data in order to map and describe the effect of coastal run-off onto the coastal areas in the Baltic Sea basin. For getting a larger range of ISPM and a larger spatial coverage, turbidity was used here to derive ISPM in the Gulf of Bothnia, and then the full data set (including the ISPM estimated from turbidity) was used to extend the range of values in order to represent a regional relationship. As the relationship of ISPM and turbidity showed a very strong correlation (Fowler et al., 1998), this approach seems justified (see Fig. 4).

The results from this study show that one can derive ISPM reliably from Sentinel 3 OLCI remotely sensed data via particle scatter (Fig. 6). ISPM derived from particle scatter had a Mean Normalized Bias of  $-24\%$  (i.e. an underestimation of ISPM), and the Root Mean Square Error was  $52\%$ , indicating a rather low relative error for a Level 2 product in optical case 2 waters (Kratzer and Vinterhav, 2010; Beltrán-Abaunza et al., 2016).

Kyryliuk and Kratzer (2019) evaluated total SPM derived from C2RCC against in situ data and found that the SPM product can be derived very reliably with a Mean Normalized Bias (MNB) of  $25\%$ , a Root Mean Square Error (RMSE) of  $73\%$  and a Mean Absolute Percentage Difference (MAPD) of  $64\%$  when applying the SPM-specific scatter in the SNAP processor and assuming a  $b_{wit}$  of  $1.72$ . These results were much better than for the current standard processor applied by EUMETSAT which showed extremely high overestimations of SPM, and thus turbidity. The retrieved turbidity had an RMSE of  $1011\%$ , a MNB of  $189\%$  and an MAPD of  $214\%$  (Plowey, 2019). By applying regional IOP's, it is possible to derive more reliable level 2 products from remote sensing data (Kyryliuk and Kratzer, 2019). In this study we applied the regional ISPM-specific scatter instead to retrieve ISPM reliably.

Figs. 7b and 8 illustrate a Baltic-wide application of the ISPM algorithm derived from particle scatter. Several coastal areas are

highlighted in Fig. 8 in order to discuss the distribution of ISPM in the near-shore vicinity. Fig. 9 shows a 6-month time-series of ISPM in the Baltic proper, indicating strong seasonal changes. The April composite clearly highlights the influence from land after snow melting causing increased run-off during spring. The images from summer also show the occurrence of filamentous cyanobacteria, which due to their gas vacuoles result in increased scatter (Dubelaar et al., 1987). In 2018, the cyanobacteria blooms were strongest during July and less prominent in August. The image from autumn also specifically highlights the influence of inorganic particles from land (similar to the image from April).

The elevated concentrations of ISPM in coastal areas show distinct regional and seasonal patterns (Fig. 8) which may be caused both by coastal run-off and by resuspension in shallow bottom areas, such as in the Väinameri Sea (VS), Estonia which has a mean water depth of only  $5$  m. Therefore, the bay is strongly influenced by resuspension of sediments caused by wind-wave stirring (Suursaar et al., 2001). As most bio-optical research groups in the Baltic Sea area only measure total SPM we will quote (total) SPM values from the literature in the comparisons below. Raag et al. (2014) and Alikas et al. (2015) quoted SPM concentrations in Estonian coastal waters ranging from  $0.75$  to  $2.60$   $g^{-3}$  in the Gulf of Finland (near Tallinn Port) and between  $10.04$  and  $24.23$   $g^{-3}$  in Pärnu bay, located in the NE Gulf of Riga (GoR) which has a mean depth of only  $23$  m (Snoeijs-Leijonmalm et al., 2017).

The Bay of Pomerania (BoP), off the shores of Germany and Poland is also very shallow coastal area with a mean depth of only  $20$  m. The Oder Bank, a sand bank (Viehberg et al., 2008) is clearly depicted by the ISPM image (Fig. 8). This may be partially because of an increase of resuspended particles due to wind as the water above the Oder bank is only about  $10$  m deep. Alternatively, the higher ISPM values could be due to bottom effects as the Secchi depth in the southern Baltic can be well above  $10$  m depth (Wasmund et al., 1998).

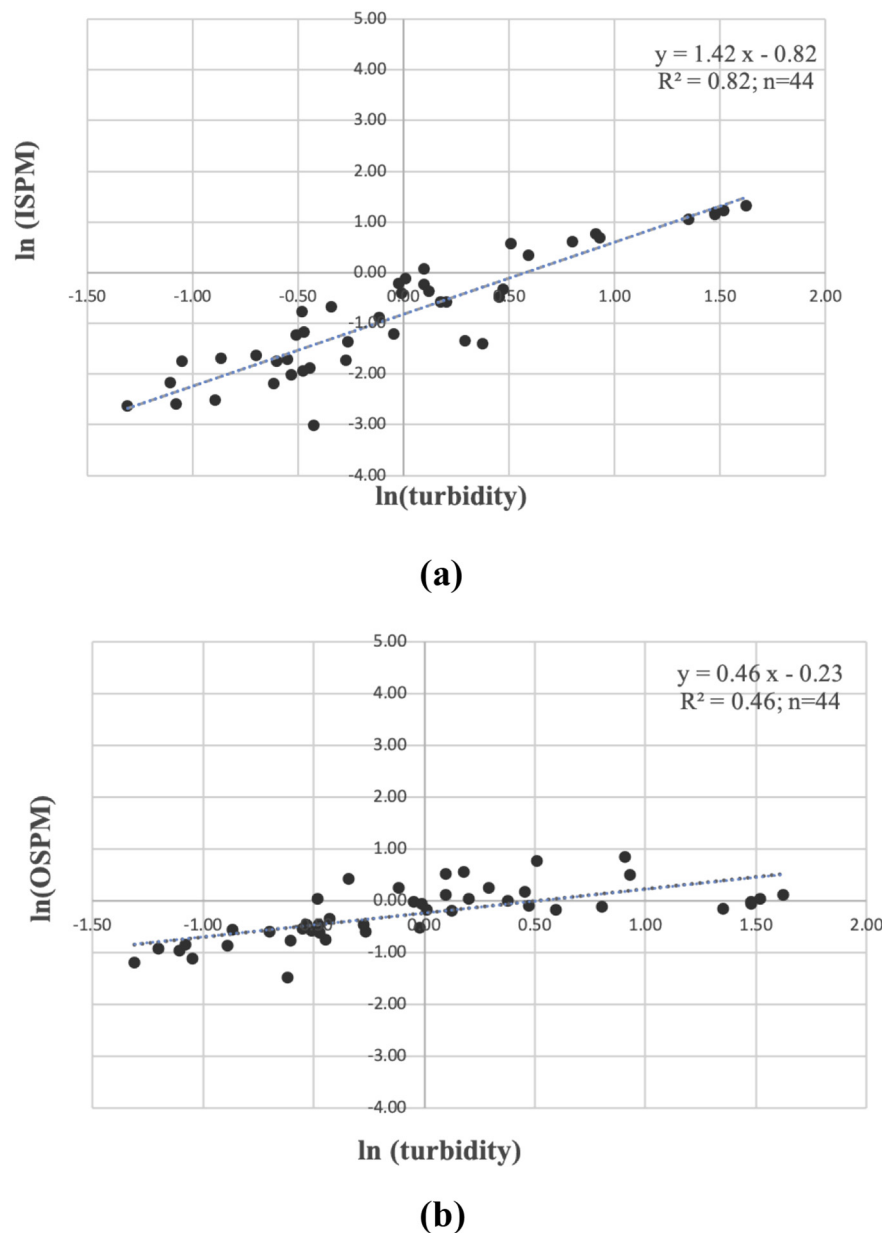


**Fig. 4.** a) The relationship between  $\ln(\text{ISPM})$  and  $\ln(\text{turbidity})$  proved to be very strong ( $R = 0.91$ ) although the data covered different times of year. The regression equation from a) was used to generate an additional ISPM data set from the Bothnian Sea and then applied together with measured ISPM data from the Baltic proper to derive the relationship between ISPM and particle scatter (Fig. 5a). b) The relationship between  $\ln(\text{OSPM})$  and  $\ln(\text{turbidity})$  showed only a moderate dependency between the two variables.

Ohde et al., 2007, measured an SPM range of  $0.5\text{--}20\text{ g}^{-3}$  in the BoP,  $0.4\text{--}5.0\text{ g}^{-3}$  in the Bornholm Sea,  $0.7\text{--}9.0\text{ g}^{-3}$  in the Arkona Sea and  $3.0\text{ to }6.0\text{ g}^{-3}$  in the Gotland Sea (including times of cyanobacteria blooms in summer).

The Bay of Gdansk (BoG) has a mean depth of 57 m (Snoeijs-Leijonmalm et al., 2017) and has a lot of coastal influence (Fig. 8). Elevated ISPM concentrations are highlighted in the extent of the plume at the mouth of the river Vistula discharging into the inner bay, loaded with inorganic particles due to river and farm land erosion. The SPM concentration in the bay varies between  $0.4$  and  $15.7\text{ g}^{-3}$  (Woźniak et al., 2011) and may also be influenced by cyanobacteria blooms in summer. The Vistula is the second largest river draining into the Baltic Sea and spring flushes usually occur in March–April due to snow and ice melting (Bukanova et al., 2018). The Vistula Lagoon south directly adjacent to the BoG is a shallow, semi-enclosed transitional water bodies. It acts as sedimentation basins for organic and inorganic matter

on its way from land to the sea (Emelyanov, 2005). The SPM concentration in the Vistula Lagoon varies from  $4$  to  $230\text{ g}^{-3}$  with a mean value of  $30\text{ g}^{-3}$  (Chubarenko, 2008). 54% of the total SPM is of biogenic origin. Wind-wave stirring in autumn can induce bottom erosion and increase the inorganic fraction to  $> 60\%$  (Chubarenko et al., 1998).

Another interesting coastal area depicted in Fig. 8 is the Curonian Lagoon (CL). The SPM concentration in the lagoon varies from  $1$  to  $138\text{ g}^{-3}$  with a mean of  $25.8\text{ g}^{-3}$  (Lukashin et al., 2017) with the Neman River discharging into the lagoon. Spring flushes occur typically in March–May, when the river approximately delivers 42% of the annual water discharge into the lagoon and the mean SPM concentration in the river mouth is  $33\text{ g}^{-3}$  (Lukashin et al., 2017). Vaičiūtė et al. (2012) quoted SPM concentrations in the lagoon ranging from  $1.05$  to  $32\text{ g}^{-3}$  with mean values of  $6.01 \pm 4.61\text{ g}^{-3}$ . Due to the high productivity in the lagoon, the biogenic component of SPM dominates, reaching up to about 74% (Chechko, 2017). The Curonian Lagoon

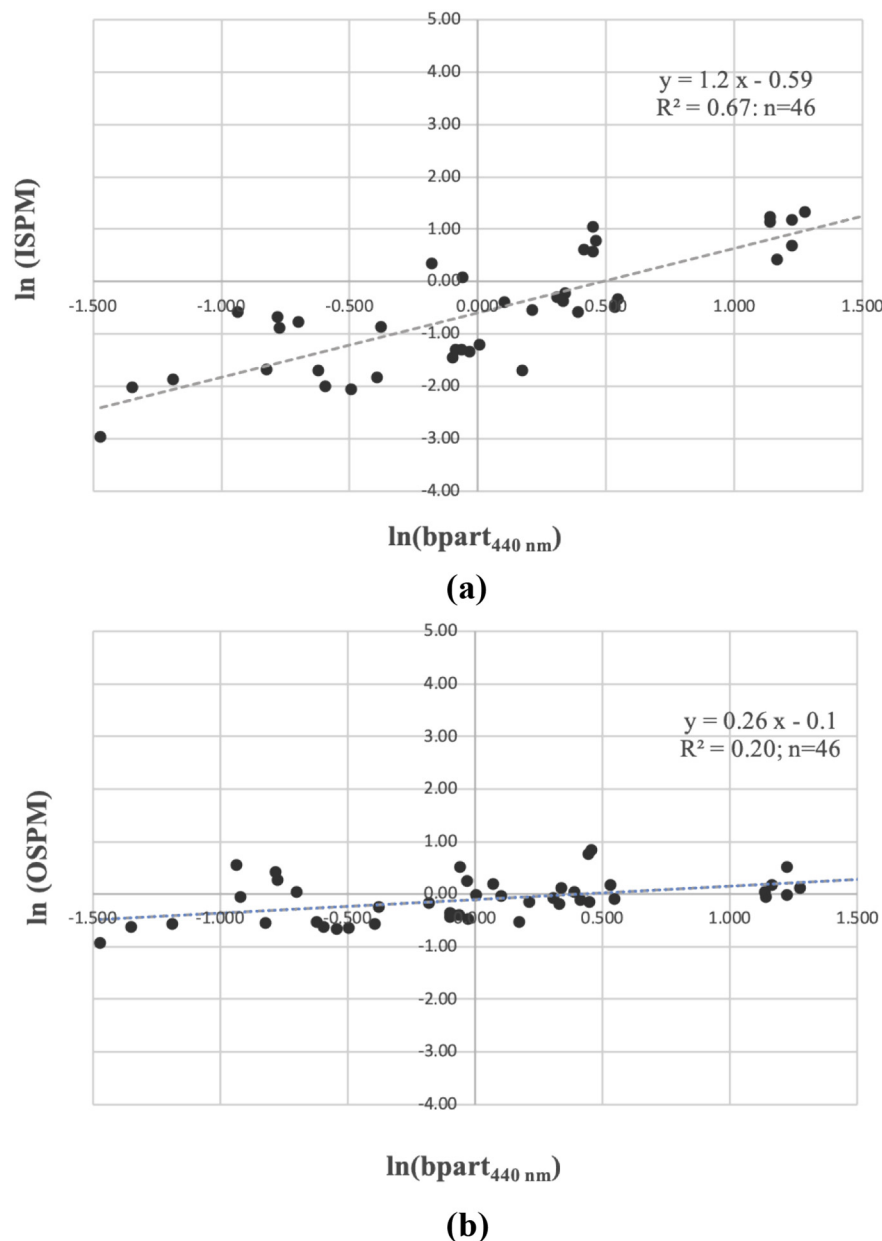


**Fig. 5.** a) The relationship between ln(ISPM) and ln(bpart<sub>440</sub>) proved to be strong although the data covered different times of year and various Baltic Sea basins. b) The relationship between ln(OSPM) and ln(turbidity) shows only modest dependency between the two variables.

discharges annually approximately 660,000 tons of SPM into the open sea through the Klaipeda Strait (Chechko, 2017; Lukashin et al., 2017). The sediment plumes and the distribution of coastal SPM are clearly visible on satellite images (Vaičiūtė et al., 2015). The ISPM concentrations along the Lithuanian and Latvian coasts (LC) highlight what appears to be a mix between the discharge from the Curonian Lagoon as well as coastal resuspension of sandy shallow bottom substrates and carried up North by the anti-clockwise rotation of water masses in the Baltic proper (Kullenberg, 1981; Stigebrandt, 2001).

Elongated coastal bays in the NW Baltic Sea such as Himmerfjärden (HF) and Bråviken (BR) bay show substantially elevated concentration of inorganic particles in the most inner part of the bays which are most strongly influenced by streams and rivers. For example in the north of Himmerfjärden bay, where Himmerfjärden (HF) connects to Lake Mälaren through a lock. During times of high precipitation, the lock is opened to release water into Himmerfjärden in order to avoid the flooding of Lake Mälaren and Stockholm city (Lagerblad, 2010). Bråviken (BR) shows very high ISPM concentration throughout the entire

bay which also causes an increase in reflectance (Fig. 3) and thus particle scatter. Most of the coastal influence is caused by the run-off from Motala River that runs through the city of Norrköping and drains into the very inner bay. There is a visible plume of ISPM extending into the open sea, way beyond the mouth of the bay (Fig. 8). The plume is further carried south by the so-called Swedish current, i.e. a net surface current along the Swedish coast caused by the anti-clockwise rotation of water masses in the Baltic proper (Kullenberg, 1981; Stigebrandt, 2001). However, the highest proportion of ISPM already falls out in the inner bay.

Additionally, elevated ISPM concentrations were observed in Swedish coastal waters at the so-called *High Coast* (HC, in Swedish: Höga kusten), highlighting the extent of two distinct river plumes (Indalsävlan and Ängermanävlan), discharging into relatively deep waters (about 200 m depth), and falling out relatively close to the coast being more rapidly diluted.

It must be pointed out, though, that the derived ISPM-b<sub>440</sub> algorithm probably does not cover the full range of values of ISPM observed

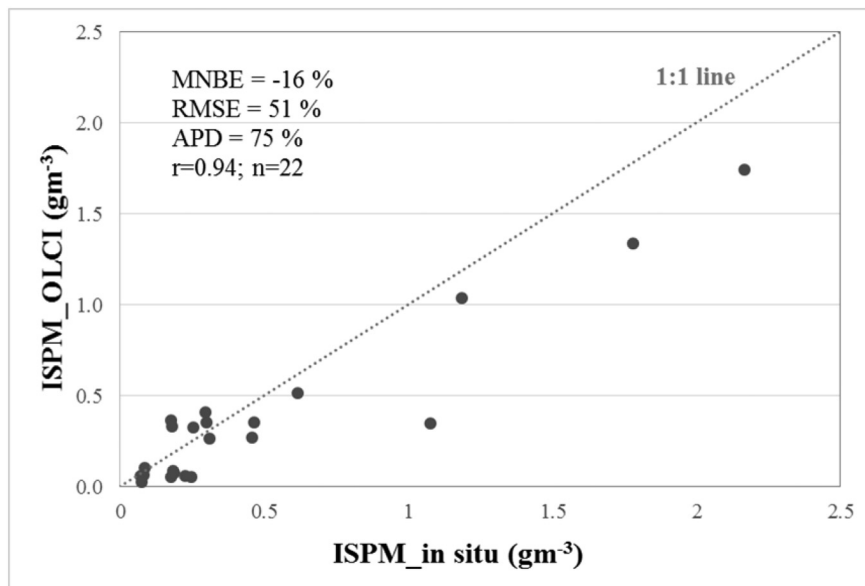


**Fig. 6.** Match-ups of ISPM generated from OLCI data plotted against ISPM measured in situ. Both ISPM (measured gravimetrically) and  $b_{440}$  (measured with an AC9, WetLabs) were measured during several dedicated optical research campaigns across the Baltic Sea and the Gulf of Bothnia in order to cover a large range of both inorganic particles and scatter. An empirical algorithm between ISPM and  $b_{440}$  (AC9) was derived from the in situ data using least squares regression analysis ( $n = 46$ ). The algorithm was then applied to OLCI  $iop\_bpart$  data processed with the C2RCC-SNAP processor. An independent data set ( $n = 22$ ) of matching in situ data was used to evaluate the satellite retrieval of ISPM. Note that all values above  $1 \text{ g}^{-3}$  were from within the inner Himmerfjärden bay.

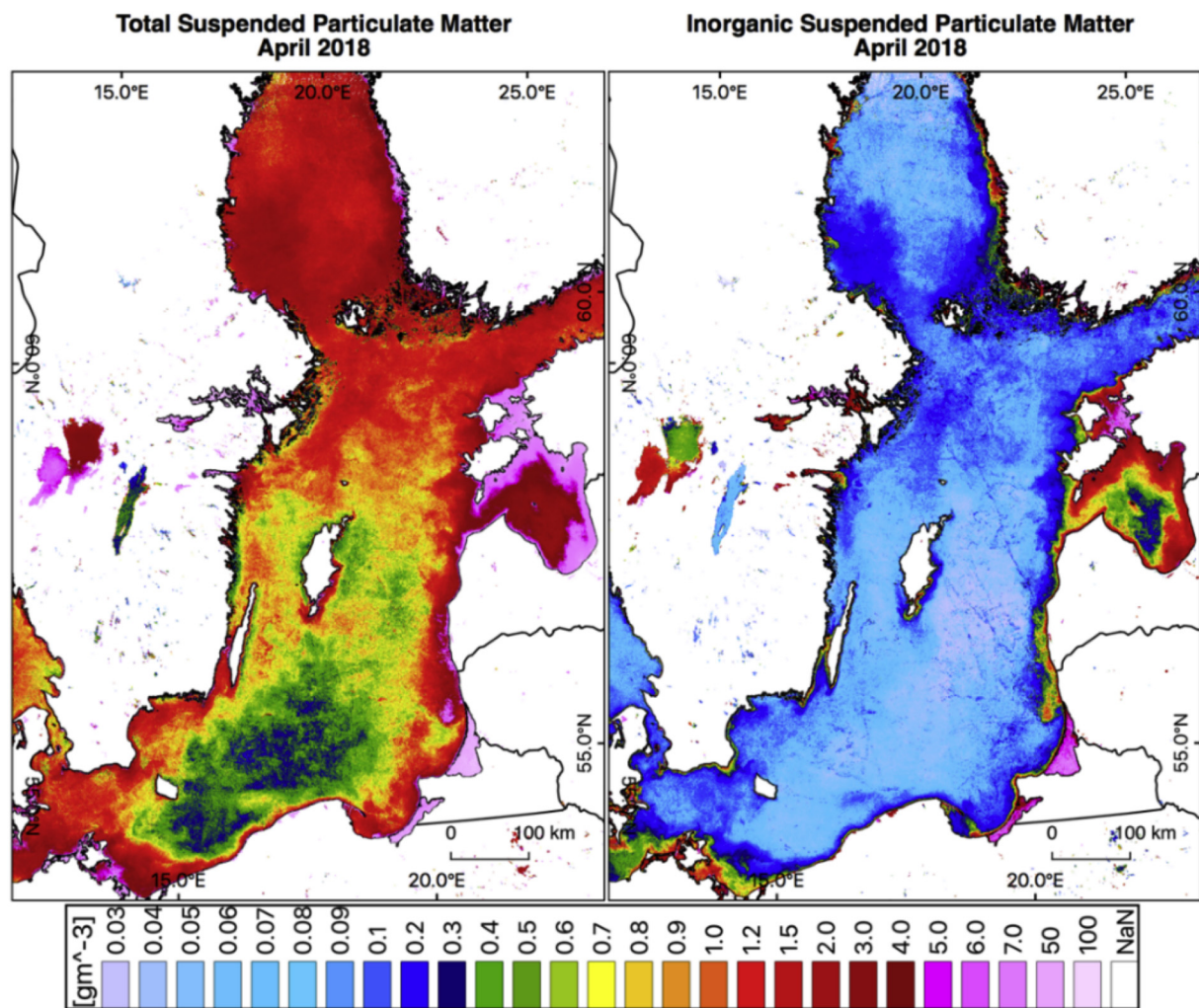
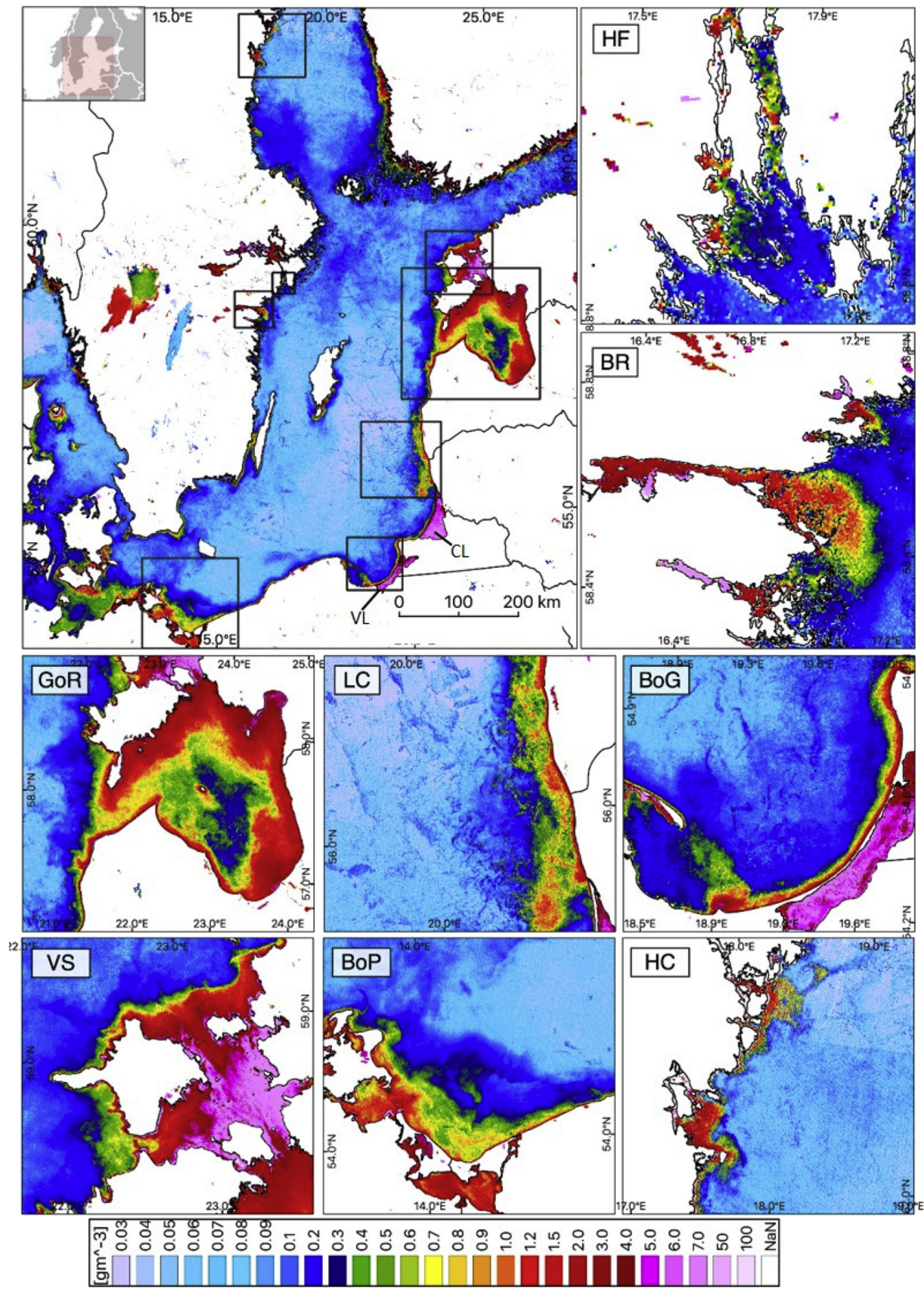


**Fig. 7.** a) A monthly composite from April 2018 of total suspended particulate matter (left) and b) inorganic suspended particulate matter (right), generated using C2RCC-SNAP and the Level-3 Binning processor applied to Sentinel-3A OLCI (Level-1b data). Country boundaries (Natural Earth; <https://www.naturalearthdata.com/downloads/10m-cultural-vectors/10m-admin-0-boundary-lines/>). The ISPM product was derived using Eq. (C). The SPM product was derived using the SPM-specific scatter from Kratzer and Moore (2018) as described in Kyrliuk and Kratzer (2019). (For interpretation of the references to color in this figure, the reader is referred to the web version of this article.)



(caption on next page)

**Fig. 8.** The empirical ISPM algorithm applied to *iop\_bpart* derived from C2RCC-SNAP. The monthly average from April 2018 was generated by ‘binning’ all available scenes. Eight coastal areas in the Baltic Sea were chosen to highlight different coastal processes, such as resuspension in the Gulf of Riga (GoR), shallow bottoms in the Väinameri Sea (VS) and resuspension and a sand bank in the Bay of Pomerania (BoP), river plumes in the Bay of Gdansk (BoG) and the Swedish High Coast (HC), coastal run-off (Himmerfjärden bay, HF) as well as the extent of river runoff in the narrow, elongated Bråviken bay (BR). The highest ISPM values are shown in the Vistula Lagoon (VL) and the Curonian Lagoon (CL) in the south-eastern Baltic (pink). (For interpretation of the references to color in this figure legend, the reader is referred to the web version of this article.)

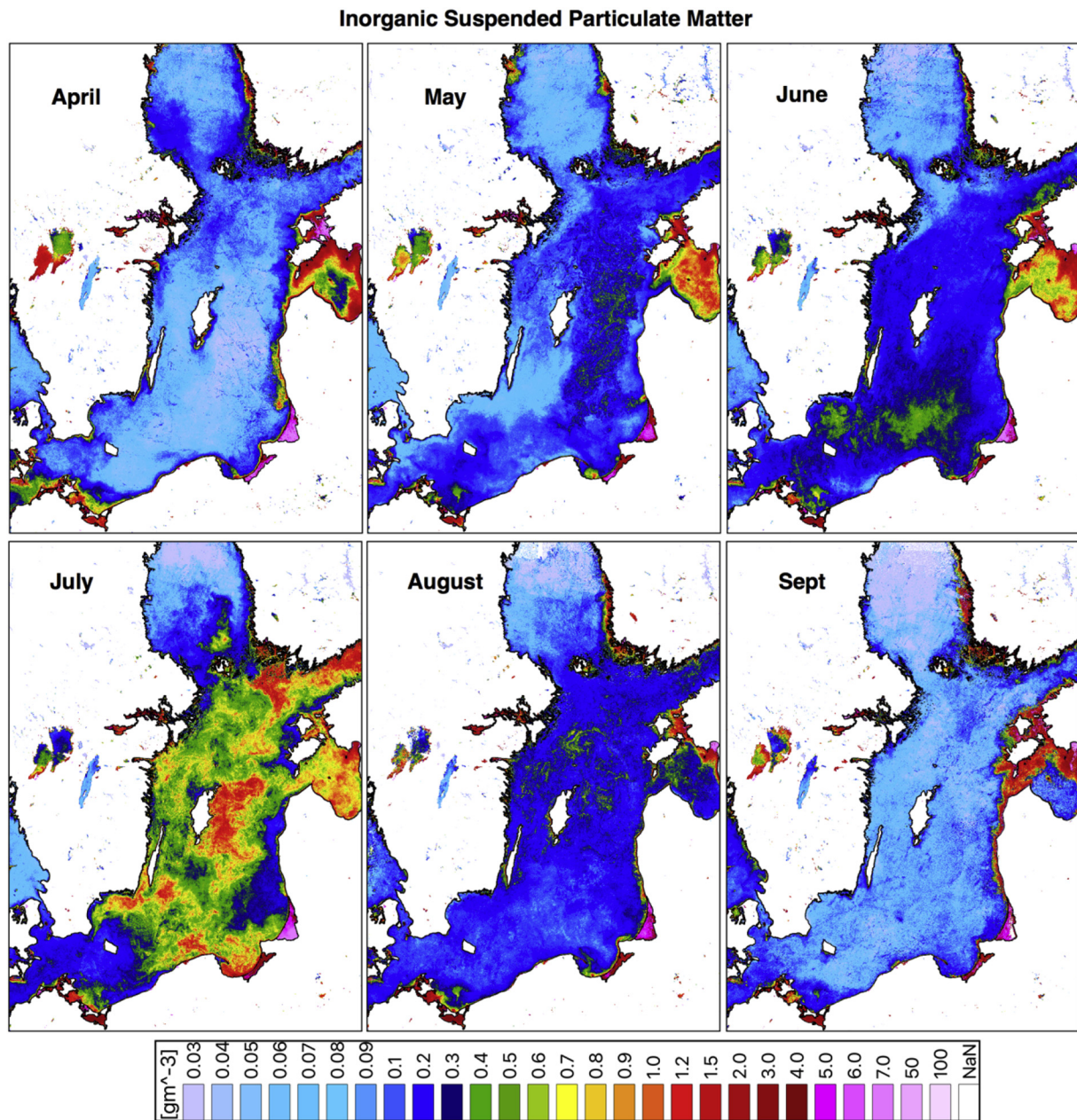


**Fig. 9.** A 6-month time-series of ISPM between April and Sept 2018 over the Baltic Sea derived from S3A OLCI C2RCC-SNAP using the ISPM algorithm. The time series covers the most productive seasons in the Baltic Sea.

in the Baltic Sea, so the algorithms should be treated with some caution at higher values (Fig. 6). However, our algorithm covered ISPM ranges of up to  $9.73 \text{ g m}^{-3}$  which is relatively high for Baltic Sea conditions, and the correlation with particle scatter was significant.

Further analysis of Fig. 6 shows that values  $> 1 \text{ mg m}^{-3}$  were underestimated by about 30% ( $n = 4$ ) while the values  $< 1 \text{ mg m}^{-3}$  were underestimated by 23% ( $n = 18$ ). As mentioned in the introduction, Kratzer and Moore (2018) found that the mean backscatter ratio for the Baltic Sea is  $0.0170 (\pm 0.0103; n = 22)$ , and that the histogram of the

backscatter ratio in the Baltic Sea is bimodal — with one peak at 0.0171, possibly corresponding to the open sea, and another peak at 0.0286, indicating brighter inner coastal waters. It is likely that the derived ISPM-b440 algorithm underestimates the higher values in inner coastal areas somewhat more because the backscatter ratio is not constant. The higher refractive index in the inner bay affects the volume scattering function, increasing the back-scatter ratio (Petzold, 1972; Mobley et al., 2002; Kratzer and Moore, 2018).

However, as the ISPM algorithm presented here is based on the

specific scatter rather than the specific backscatter, it thus will underestimate the higher ISPM values. There may also be some interference from land adjacency affects in the inner bay which would seemingly increase the derived ISPM values. Another factor to consider is the parameterization of  $b_{wit}$ . It is possible that a factor of  $b_{wit} = 1.72$  attributes a too high proportion of the scatter towards white scatterers, which will then give an overall underestimation of particle scatter, both in the lower and the higher ISPM ranges. Thus, for the Baltic Sea,  $b_{wit}$  may have to be reduced in C2RCC somewhat in order to improve the retrieval of both ISPM and SPM.

#### 4.1. Influence on under-water light conditions and ecology

The coastal in situ transects of ISPM shown in Fig. 2a and b clearly illustrate how the ISPM concentrations decrease from the very inner bay out to the open sea. Using a coastal model based on all optical constituents Kratzer and Tett (2009) identified ISPM as an indicator for coastal waters and showed that the values converge towards zero at about 15 km off-shore. In the current study a larger number of transects was included, and they confirmed the general trend of decreasing ISPM inside the bay and converging towards a median value of  $0.17 \text{ g}^{-3}$  at Stations BIII and BY31. This confirms that Landsort Deep acts as a sink of inorganic particulate matter, while the inner bay acts as a source with values reaching up to ca.  $3.6 \text{ g}^{-3}$ . Using multiple regression analysis Kratzer and Tett (2009) could show that ISPM scatter contributes with about 20% to the diffuse attenuation of light at 490 nm ( $K_d(490)$ ) in the very inner bay while CDOM absorption contributes with about 50%. This means that in inner coastal waters ISPM has a more than significant influence onto the diffuse attenuation of light.  $K_d(490)$  correlates very strongly to  $K_d(PAR)$ , the diffuse attenuation coefficient of photosynthetically active radiation (Kratzer et al., 2003; Pierson et al., 2008) and thus also affects the maximum growth depth of macroalgae (Kautsky et al., 1986).

Andersson et al. (2018) have shown that in inner estuaries, CDOM may limit pelagic primary production, and Fig. 2a and b indicate that ISPM in the inner bay is generally very high and also variable. It thus will also have a significant effect on light attenuation, and thus productivity, especially during the spring. Kari et al. (2018) showed that the progression of the phytoplankton spring bloom often starts in the middle of the bay, which may well be related to the light limitation of phytoplankton induced by the high CDOM absorption combined with the high inorganic particle scatter in the inner bay and by the effect of ice thawing. Himmerfjärden bay consists of a series of basins that are each separated by a sill. The water circulation is estuarine with a relatively low freshwater input (Engqvist and Omstedt, 1992; Engqvist and Stenström, 2009) both from small local streams and from Lake Mälaren which is connected to the bay through a lock in Södertälje. The water retention time in the surface waters is about 20 days (Håkanson and Stenström-Khalili, 2010). The internal circulation inside each basin may trap larger particles which then fall out in the inner basins while smaller particles (i.e. clay and silt) are transported over the sill into the next basin, in a cascade-like manner, and eventually out into the open sea. B1 at about 30 km off-shore (Fig. 2) lies only about 4 km offshore and is therefore still influenced by coastal processes (Kratzer and Tett, 2009) as indicated by the somewhat elevated levels at B1 just outside the bay compared to the other open sea stations. Fig. 2a shows that in spring, there is a large spatial trend of ISPM in the inner bay, although with a large variability due to strong fluctuations in run-off. During summer (Fig. 2b) the fluctuations in the inner bay are much less. The slightly increased ISPM values outside the bay at about 20–25 km off-shore may be caused by the influence from coastal upwelling which is quite frequent in the Baltic Sea at about 10–20 km offshore during the summer period (Gidhagen, 1987).

During summer, the median ISPM concentration is about 50% lower in the open sea than during the spring period (Fig. 2b). This may be linked to the higher run-off during spring after the ice thawing and

possibly also to the high frequency of diatoms during the phytoplankton spring bloom. Diatoms have spines that keep them longer in suspension, and they also produce frustules made from silica that contribute to the inorganic fraction of the suspended matter.

The ISPM image shown in Figs. 7b and 8 confirm the results from the in-water transects and shows that the highest concentrations of ISPM are found in near-coastal areas and inner bays. The same is true for total SPM, which however, is carried much further off-shore (Fig. 7), presumably because organic matter is relatively light compared to ISPM consisting of sand, silt and mud particles.

Bowers and Binding (2006) pointed out that ISPM binds up with organic SPM, which increases the buoyancy. Fine mineral particles are bound together with organic material to flocs (Eisma et al., 1990) which allows also for inorganic particles to be carried further off-shore. However, the images in Figs. 7b and 8 indicate, that most of the inorganic particles in the Baltic Sea fall out in near-coastal areas and inside the bays. Reader et al. (2019) pointed out that mixed sandy sediments are usually found near the shore while mud sediments are more characteristic for the off-shore waters in the Gdansk Deep presumably because they are lighter and thus can be carried further off-shore.

Phytoplankton is also counted as part of SPM and is also found much further off-shore (note that the word *plankton* is Greek and means *wanderer*). The Gulf of Bothnia and the Gulf of Finland have relatively high concentration of total SPM in the inner parts, while the southern Baltic Sea, especially the Bornholm and Arkona basins seem to act as sinks of SPM. It must be noted that the SPM composite image from spring 2018 (Fig. 7a) includes the peak of the phytoplankton spring bloom in the NW Baltic proper which was measured during our field campaigns in mid-late April (Kyryliuk and Kratzer, 2019). In the Bothnian Sea the peak of the spring bloom usually occurs somewhat later, i.e. during May. During the spring cruise in May 2018 there was still a large ice sheet in the Råneå area and the highest measured Chl-a concentration ( $8.91 \mu\text{g l}^{-1}$ ) during the spring cruise in the Gulf of Bothnia was measured further down south at the Swedish High Coast on 14 May 2018, indicating a spring bloom at the coastal station. This means that the high SPM concentration in the Gulf of Bothnia in Fig. 3) most likely indicate the influence of organic matter and phytoplankton in the open sea as well as very high inorganic matter concentrations in coastal areas (Figs. 7b and 8) during the ice thawing period. It is likely that the high CDOM concentrations measured in the Bothnian Sea (Fig. 3) are a limiting factor for the light penetration, and therefore contribute to the late occurrence of the spring bloom. The ISPM time-series (Fig. 9) shows that due to light scattering properties of internal gas vacuoles in filamentous cyanobacteria the onset of the development of the summer bloom can be tracked already in May and June in the Eastern Gotland Basin using the ISPM product. Due to their internal gas vacuoles the cyanobacteria increase the total backscatter, which in the case of the open Baltic Sea indicates filamentous cyanobacteria in summer. Although this is clear evidence of the limitation of the algorithm to detect inorganic matter, it also shows the possibility of early detection of filamentous cyanobacteria blooms in the open Baltic Sea during early summer. Kratzer and Tett (2009) have shown that inorganic matter tends towards zero in the open Baltic Sea, while it shows a polynomial increase towards the coast. In August 2018 the cyanobacterial bloom decreased substantially (green structures in the open sea, Fig. 9) indicating the end of the summer cyanobacterial bloom. This suggests, that the ISPM product can also be used to identify the onset and decay of filamentous cyanobacteria in the Baltic Sea during summer. Fig. 9 shows the first signs of such a bloom in the May composite image, which is rather early. It is likely that the onset of the blooms were shifted towards the second half of May as Kahru and Elmgren (2014) have shown that the centre of timing of the cyanobacteria bloom occurrence has been shifted forward by 20 days over during a period of 35 years (1979–2013), towards approximately the 19 July of the respective year. This means that the onset of the bloom is also likely to be shifted forward in time, as indicated in the monthly

means in Fig. 9. It must be pointed out that 2018 was an exceptionally warm year (both during spring and summer), which may explain the occurrence of blooms already in May.

Strictly speaking only the images from spring and autumn represent ISPM in the coastal zone while in summer both coastal ISPM and filamentous cyanobacteria occur and may influence the ISPM product. There are, however, specialized image analysis tools such as pattern recognition analysis which can be used to distinguish between the two phenomena (Miller et al., 2006).

The very high concentration of ISPM in coastal areas will not only affect the productivity (as discussed above), but may also influence the behaviour of fish and their choice of reproductive areas. It is generally known, that small fish often hide in between macroalgae in order to avoid being caught by predators. Some fish species are also known to change their mating behaviour with changing turbidity and silting. Järvenpää and Lindström (2004) found that increased turbidity can change the mating behaviour of the sand goby, *Pomatoschistus minutus* (Pallas) and decrease the opportunity for sexual selection as well as selection intensity. Ajemian et al. (2015) found that sticklebacks responded to predator presence by significantly increasing use of sheltered habitats. Veneranta et al. (2011) evaluated the distribution and extent of the reproduction areas of pikeperch, *Sander lucioperca* (L.), in the northern Baltic Sea using a geographic information system (GIS)-based predictive spatial distribution model. The results indicated that pikeperch reproduction areas are located in the innermost coastal areas where high water turbidity explained best their presence. The authors suggested the use of remote sensing data is a cost-effectively way to validate their distribution model and to extend the survey spatially to cover more coastal areas. Here, Sentinel-2 data would be of especially high value due to its improved spatial resolution (10–60 m) when compared to Sentinel-3 (Toming et al., 2016).

## 5. Conclusions

We present here a novel Baltic Sea algorithm to derive ISPM from particle scatter at 440 nm. The regression model showed to be significant and is based on an in situ data set covering a relatively large range of ISPM, thus making the case for a regional algorithm. The validation data set showed that there was no significant difference between the data measured in situ and predicted by OLCI. The standard error of the derived OLCI match-up data was only 10%, and was thus within the goal of the mission requirements of Sentinel-3.

Both the in situ measurements as well as the satellite data demonstrate that most of the inorganic particles fall out rather close to the coast (within the order of tens of kilometres), apart from in very shallow areas where wind-wave stirring leads to the resuspension of inorganic particles. The open Baltic Sea, on the other hand, acts as a sink of inorganic particles. The ISPM images indicate resuspension in shallow bays as well as coastal run-off from rivers and streams, as well as possible bottom effects in very shallow areas.

ISPM is likely to limit phytoplankton production in inner coastal bays and archipelagos, and has also been shown to influence the reproductive behaviour of fish. With the advances in ocean colour remote sensing it is possible to derive large-scale information on turbidity with improved spatial and temporal resolution compared to traditional sampling and monitoring methods. This helps to improve our understanding of coastal dynamics as well as biology and ecology. The derived algorithm is also applicable to the MERIS data archive (2002–2012) and thus could be used to evaluate long-term changes in river run-off e.g. caused by climate change.

As ISPM images from late spring and summer (May–August) may be affected by the presence of filamentous cyanobacteria (containing gas vacuoles) we recommend the use of monthly composites from April for the long-term assessment of the extent of coastal run-off as to avoid the interference of cyanobacteria blooms in the images. Alternatively, pattern recognition techniques could be applied to distinguish between

coastal run-off and off-shore production of filamentous cyanobacteria during summer.

ISPM is an important ecological state variable influencing primary as well as secondary producers and can be derived reliably from space. We therefore would like to recommend to HELCOM and the national monitoring programs around the Baltic Sea to introduce ISPM measurements in the in situ monitoring programs. This will also allow to test and extend the viability of the ISPM algorithm to cover the full range of concentrations measured in coastal areas.

## Author contributions

The in situ data was measured and analysed by Susanne Kratzer with help by various members of the marine remote sensing group at Stockholm University during field campaigns and in the laboratory. Susanne Kratzer also derived the in-water algorithms and analysed the match-up data and wrote most of the manuscript. Dmytro Kyryliuk analysed the remote sensing data and contributed to the writing. Carsten Brockmann provided support in the choice of remote sensing flags and contributed to the introduction and the methods section and to the final version of the manuscript.

## Funding

This research was funded by the Swedish National Space Agency (Dnr. 147/12) and by the European Space Agency (ESA/ESRIN project 12352/08/I-OL) and the ESA MERIS 4th Reprocessing contract to ARGANS Ltd., UK (Ref 4000111320/14/I-LG, WP1). The Swedish Agency for Water and Marine Management as well as County Board Norrbotten provided co-funding within the EU Interreg Nord project SEAmBOTH (contract no. 502-14063-2017).

## Declaration of competing interest

The authors declare no conflict of interest. Any role of the funding sponsors in the choice of research project; design of the study; in the collection, analyses or interpretation of data; in the writing of the manuscript; or in the decision to publish the results.

## Acknowledgments

Great thanks to Gerald Moore, Therese Harvey, José Maria Beltrán-Abaunza, Elina Kari, Sélima Ben Mustapha, Evgeny Morozov, Matthew Plowey, Eeva Bruun, and Noora Haavisto for help in the field and/or in the lab. Thanks to the marine monitoring group at Umeå University and the Swedish Coast Guards on KBV181 for great support during field work. We would also like to thank the reviewers who all contributed to a substantial improvement of the manuscript.

## References

- ESA, 2007. In: Drinkwater, Mark R., Rebhan, Helge (Eds.), Sentinel-3 Mission Requirements Document, 2nd edition. Ref. No. EOP-SMO/1151/MD. 19 February 2007. [https://earth.esa.int/c/document\\_library/get\\_file?folderId=13019&name=DLFE-799.pdf](https://earth.esa.int/c/document_library/get_file?folderId=13019&name=DLFE-799.pdf) (last accessed on 4 November 2019).
- Kirk, J.T.O., 2011. Light and Photosynthesis in Aquatic Ecosystems, 3rd ed. Cambridge University Press, New York, NY, USA 1984; pp. 524, ISBN 978-0-521-15175-7.
- Kyryliuk, D., Kratzer, S., 2019. Evaluation of Sentinel-3A OLCI products derived using the Case-2 Regional CoastColour Processor over the Baltic Sea. *Sensors* 19 (16), 3609.
- NOMAD NASA Bio-optical Marine Algorithm Dataset. Available online: <https://seabass.gsfc.nasa.gov/wiki/NOMAD> (accessed on 16 October 2019).
- ESA SNAP Earth Observations and Science Tools. Available online: <http://step.esa.int/main/toolboxes/snap/> (accessed on 16 October 2019).
- Ajemian, M.J., Sohel, S., Mattila, J., 2015. Effects of turbidity and habitat complexity on antipredator behavior of three-spined sticklebacks (*Gasterosteus aculeatus*). *Environ. Biol. Fish* 98 (1), 45–55.
- Alikas, K., Kratzer, S., 2017. Improved retrieval of Secchi depth for optically-complex waters using remote sensing data. *Ecol. Indic.* 77, 218–227.
- Alikas, K., Kratzer, S., Reinart, A., Kauer, T., Paavel, B., 2015. Robust remote sensing algorithms to derive the diffuse attenuation coefficient for lakes and coastal waters.

- Limnology and Oceanography Methods 13 (8), 402–415.
- Andersson, A., Brugel, S., Paczkowska, J., Rowe, O.F., Figueroa, D., Kratzer, S., Legrand, C., 2018. Influence of allochthonous dissolved organic matter on pelagic basal production in a northerly estuary. *Estuar. Coast. Shelf Sci.* 204, 225–235.
- Arnone, R.A., Wood, A.M., Gould, R.W., 2004. The evolution of optical water mass classification. *Oceanography* 17 (2), 14–15.
- Attila, J., Koponen, S., Kallio, K., Lindfors, A., Kaitala, S., Ylösto, P., 2013. MERIS Case II water processor comparison on coastal sites of the northern Baltic Sea. *Remote Sens. Environ.* 128, 138–149.
- Beltrán-Abaunza, J.M., Kratzer, S., Högländer, H., 2016. Using MERIS data to assess the spatial and temporal variability of phytoplankton in coastal areas. *Int. J. Remote Sens.* 1–25.
- Blondeau-Patissier, D., Schroeder, T., Brando, V., Maier, S., Dekker, A., Phinn, S., 2014. ESA MERIS 10-year mission reveals contrasting phytoplankton bloom dynamics in two tropical regions of northern Australia. *Remote Sens.* 6 (4), 2963–2988. <https://doi.org/10.3390/rs6042963>.
- Boss, E., Pegau, W.S., Lee, M., Twardowski, M., Shybanov, E., Korotaev, G., Baratange, F., 2004. Particulate backscattering ratio at LEO 15 and its use to study particle composition and distribution. *Journal of Geophysical Research: Oceans (C1)*, 109.
- Bowers, D.G., Binding, C.E., 2006. The optical properties of mineral suspended particles: a review and synthesis. *Estuar. Coast. Shelf Sci.* 67 (1–2), 219–230.
- Brockmann, C., Doerffer, R., Peters, M., Kerstin, S., Embacher, S., Ruescas, A., 2016. Evolution of the C2RCC neural network for Sentinel 2 and 3 for the retrieval of ocean colour products in normal and extreme optically complex waters. In: *Proceedings of the Living Planet Symposium*. Prague, Czech Republic, 9–13 May 2016. 740. pp. 54.
- Bukanova, T., Kopelevich, O., Vazulya, S., Bubnova, E., Sahling, I., 2018. Suspended matter distribution in the south-eastern Baltic Sea from satellite and in situ data. *Int. J. Remote Sens.* 39 (24), 9317–9338.
- Campbell, J., Blaisdell, J., Darzi, M., 1996. Level-3 SeaWiFS data products: spatial and temporal binning algorithms. 9 (43), 952.
- Chechko, V.A., 2017. Features of modern sedimentation process in Vistula and Curonian lagoons. In: Lisitzyn, A.P. (Ed.), *The Baltic Sea System*. Scientific World, Moscow, pp. 373–380.
- Chubarenko, B., 2008. The Vistula lagoon. In: Chubarenko, B. (Ed.), *Transboundary Waters and Basins in the South-east Baltic*. Terra Baltica, Kaliningrad, pp. 37–57.
- Chubarenko, B.V., Kuleshov, A.F., Chechko, V.A., 1998. Field study of spatial-temporal variability of suspended substances and water transparency in Russian part of Vistula lagoon. *Monographs in System Ecology* 2, 12–17.
- Cristina, S.V., Goela, P., Icely, J.D., Newton, A., Fragoso, B., 2009. Assessment of water-leaving reflectances of oceanic and coastal waters using MERIS satellite products off the southwest coast of Portugal. *J. Coast. Res.* 1479–1483.
- Dierrsen, H.M., Kudela, R.M., Ryan, J.P., Zimmerman, R.C., 2006. Red and black tides: quantitative analysis of water-leaving radiance and perceived color for phytoplankton, colored dissolved organic matter, and suspended sediments. *Limnol. Oceanogr.* 51 (6), 2646–2659.
- Doerffer, R., 2002. Protocols for the validation of MERIS water products. In: *ESA Publication PO-TN-MEL-GS-0043*. v.1.3.5. GKSS, Forschungszentrum, Geesthacht, Germany, pp. 1–42.
- Doerffer, R., Schiller, H., 2007. The MERIS Case 2 water algorithm. *Int. J. Remote Sens.* 28, 517–535. <https://doi.org/10.1080/01431160600821127>.
- Doerffer, R., Sorensen, K., Aiken, J., 1999. MERIS potential for coastal zone applications. *Int. J. Remote Sens.* 20 (9), 1809–1818. <https://doi.org/10.1080/014311699212498>.
- Dogliotti, A.I., Ruddick, K.G., Nechad, B., Doxaran, D., Knaeps, E., 2015. A single algorithm to retrieve turbidity from remotely-sensed data in all coastal and estuarine waters. *Remote Sens. Environ.* 156, 157–168.
- Dubelaar, G.B.J., Visser, J.W.M., Donze, M., 1987. Anomalous behaviour of forward and perpendicular light scattering of a cyanobacterium owing to intracellular gas vacuoles. *Cytometry* 8, 405–412. <https://doi.org/10.1002/cyto.990080410>.
- Eisma, D., Schuhmacher, T., Boekel, H., Van Heerwaarden, J., Franken, H., Laan, M., Vaars, A., Eijgenraam, F., Kalf, J., 1990. A camera and image-analysis system for in situ observation of flocs in natural waters. *Neth. J. Sea Res.* 27 (1), 43–56.
- Emelyanov, E.M., 2005. *The Barrier Zones in the Ocean*. Springer-Verlag, New York, Heidelberg.
- Engqvist, A., Omstedt, A., 1992. Water exchange and density structure in a multi-basin estuary. *Cont. Shelf Res.* 12, 1003–1026.
- Engqvist, A., Stenström, P., 2009. Flow regimes and long-term water exchange of the Himmerfjärden estuary. *Estuar. Coast. Shelf Sci.* 83, 159–174.
- Fowler, J., Cohen, L., Jarvis, P., 1998. *Practical Statistics for Field Biology*. John Wiley & Sons, Chichester.
- Gidhagen, L., 1987. Coastal upwelling in the Baltic Sea — satellite and in situ measurements of sea-surface temperatures indicating coastal upwelling. *Estuarine Coastal and Shelf Science* 24, 449–462.
- Graham, J.J., 1966. Secchi disc observations and extinction coefficients in the Central and Eastern North Pacific Ocean. *Limnol. Oceanogr.* 11 (2), 184–190.
- Håkanson, L., Stenström-Khalili, M.I., 2010. How important are local nutrient emissions to eutrophication in coastal areas compared to fluxes from the outside sea? A case study using data from the Himmerfjärden bay in the Baltic Proper. In: Friedman, A.G. (Ed.), *Lagoons: Biology, Management and Environmental Impact*. Nova Science Publisher, Inc., New York, United States, pp. 1–6.
- Harvey, E.T., Kratzer, S., Philipson, P., 2015. Satellite-based water quality monitoring for improved spatial and temporal retrieval of chlorophyll-a in coastal waters. *Remote Sens. Environ.* 158, 417–430. <https://doi.org/10.1016/j.rse.2014.11.017>.
- Harvey, E.T., Walve, J., Andersson, A., Karlson, B., Kratzer, S., 2019. The effect of optical properties on Secchi depth and implications for eutrophication management. *Front. Mar. Sci.* 5, 496. <https://doi.org/10.3389/fmars.2018.00496>.
- Järvenpää, M., Lindström, K., 2004. Water turbidity by algal blooms causes mating system breakdown in a shallow-water fish, the sand goby *Pomatoschistus minutus*. *Proc. R. Soc. Lond. Ser. B Biol. Sci.* 271 (1555), 2361–2365.
- Kahru, M., Elmgren, R., 2014. Multidecadal time series of satellite-detected accumulations of cyanobacteria in the Baltic Sea. *Biogeosciences* 11 (13), 3619.
- Kari, E., Kratzer, S., Beltrán-Abaunza, J.M., Harvey, E.T., Väiçūtė, D., 2017. Retrieval of suspended particulate matter from turbidity-model development, validation, and application to MERIS data over the Baltic Sea. *Int. J. Remote Sens.* 38 (7), 1983–2003.
- Kari, E., Merkouriadi, I., Walve, J., Leppäranta, M., Kratzer, S., 2018. Development of under-ice stratification in Himmerfjärden bay, North-Western Baltic proper, and their effect on the phytoplankton spring bloom. *J. Mar. Syst.* 186, 85–95.
- Kautsky, N., Kautsky, H., Kautsky, U., Waern, M., 1986. Decreased depth penetration of *Fucus vesiculosus* (L.) since the 1940's indicates eutrophication of the Baltic Sea. *Mar. Ecol. Prog. Ser.* 28 (1), 1–8.
- Kirk, J.T.O., 1976. Yellow substance (gelbstoff) and its contribution to the attenuation of photosynthetically active radiation in some inland and coastal southeastern Australian waters. *Aus. J. Mar. Freshw. Res.* 27, 61–71.
- Kratzer, S., 2000. *Bio-optical Studies of Coastal Waters*. PhD thesis; monograph in English. School of Ocean Sciences, University of Wales, Bangor (UWB), UK Peer reviewed. ISNI 0000 0001 3602 4205.
- Kratzer, S., Moore, G., 2018. Inherent optical properties of the Baltic Sea in comparison to other seas and oceans. *Remote Sens.* 10 (3), 418.
- Kratzer, S., Tett, P., 2009. Using bio-optics to investigate the extent of coastal waters a Swedish case study. *Hydrobiologia* 629, 169–186.
- Kratzer, S., Vinterhav, C., 2010. Improvement of MERIS data in Baltic Sea coastal areas by applying the Improved Contrast between Ocean and Land processor (ICOL). *Oceanologia* 51 (4), 1–26.
- Kratzer, S., Håkansson, B., Sahlin, C., 2003. Assessing Secchi and photic zone depth in the Baltic Sea from space. *Ambio* 32 (8), 577–585.
- Kratzer, S., Brockmann, C., Moore, G., 2008. Using MERIS full resolution data to monitor coastal waters — a case study from Himmerfjärden, a fjord-like bay in the north-western Baltic Sea. *Remote Sens. Environ.* 112 (5), 2284–2300. <https://doi.org/10.1016/j.rse.2007.10.006>.
- Kullenberg, G., 1981. *Physical oceanography*. In: Voipio, A. (Ed.), *The Baltic Sea*. Elsevier Oceanography Series 30. Elsevier, New York, pp. 418.
- Kyryliuk, D., 2014. *Total Suspended Matter Derived from MERIS Data as an Indicator of Coastal Processes in the Baltic Sea*. Masters project (examensarbete, 30 ECTS), DEEP. Stockholm University. <https://su.diva-portal.org/smash/get/diva2:1060672/FULLTEXT01.pdf>.
- Lagerblad, L., 2010. Klimatförändringar och Mälaren ur ett vatten- och naturmiljöperspektiv (Climate change in Lake Mälaren from a water and environmental perspective, in Swedish). In: *Rapport 2011:2. Avdelningen för samhällsskydd och beredskap. Länsstyrelsen i Stockholms län*. ISBN: 978-91-7281-407-3.
- Lukashin, V.N., Krechik, V.A., Klyuvitkin, A.A., Starodymova, D.P., Kochenkova, A.I., 2017. Riverine discharge and marginal filters of rivers. In: Lisitzyn, A.P. (Ed.), *The Baltic Sea System*. Scientific World, Moscow, pp. 189–214.
- Miller, P.I., Shutler, J.D., Moore, G.F., Groom, S.B., 2006. SeaWiFS discrimination of harmful algal bloom evolution. *Int. J. Remote Sens.* 27 (11), 2287–2301.
- Mobley, C.D., Sundman, L.K., Boss, E., 2002. Phase function effects on oceanic light fields. *Appl. Opt.* 41, 1035–1050. <https://doi.org/10.1364/AO.41.001035>.
- Mueller, J.L., Austin, R.W., 1995. Ocean optics protocols for SeaWiFS validation, revision 1. *Oceanogr. Lit. Rev.* 9 (42), 805.
- Nechad, B., Ruddick, K.G., Park, Y., 2010. Calibration and validation of a generic multisensor algorithm for mapping of total suspended matter in turbid waters. *Remote Sens. Environ.* 114 (4), 854–866.
- Odermatt, D., Gitelson, A., Brando, V.E., Schaepman, M., 2012. Review of constituent retrieval in optically deep and complex waters from satellite imagery. *Remote Sens. Environ.* 118, 116–126.
- Ohde, T., Siegel, H., Gerth, M., 2007. Validation of MERIS Level-2 products in the Baltic Sea, the Namibian coastal area and the Atlantic Ocean. *Int. J. Remote Sens.* 28 (3–4), 609–624.
- Petzold, T.J., 1972. *Volume Scattering Functions for Selected Natural Waters*. Scripps Institution of Oceanography La Jolla Ca Visibility Laboratory, San Diego, CA, pp. 77 No. SIO-REF-72-78.
- Pierson, D., Kratzer, S., Strömbeck, N., Håkansson, B., 2008. Relationship between the attenuation of downwelling irradiance at 490 nm with the attenuation of PAR (400 nm–700 nm) in the Baltic Sea. *Remote Sens. Environ.* 112 (3), 668–680.
- Plowey, M.D., 2019. *A Multi-scale Approach to Monitoring the Optically Complex Coastal Waters of the Baltic Sea — A Comparison of Satellite, Mooring, and Ship-based Monitoring of Ocean Colour*. Masters project (examensarbete, 60 ECTS), DEEP. Stockholm University.
- Raag, L., Sipelgas, L., Uiboupin, R., 2014. Analysis of natural background and dredging-induced changes in TSM concentration from MERIS images near commercial harbours in the Estonian coastal sea. *Int. J. Remote Sens.* 35, 6764–6780.
- Reader, H.E., Thoms, F., Voss, M., Stedmon, C.A., 2019. The influence of sediment-derived dissolved organic matter in the Vistula River Estuary/Gulf of Gdansk. *Journal of Geophysical Research: Biogeosciences* 124 (1), 115–126.
- Schiller, H., Doerffer, R., 1999. Neural network for emulation of an inverse model operational derivation of Case II water properties from MERIS data. *Int. J. Remote Sens.* 20 (9), 1735–1746.
- Schroeder, T., Behnert, I., Schaale, M., Fischer, J., Doerffer, R., 2007a. Atmospheric correction algorithm for MERIS above case-2 waters. *Int. J. Remote Sens.* 28, 1469–1486.
- Schroeder, T., Schaale, M., Fischer, J., 2007b. Retrieval of atmospheric and oceanic properties from MERIS measurements: a new Case-2 water processor for BEAM. *Int. J.*

- Remote Sens. 28, 5627–5632.
- Snoeijs-Leijonmalm, P., Schubert, H., Radziejewska, T. (Eds.), 2017. Biological Oceanography of the Baltic Sea. Springer Science & Business Media, pp. 30.
- Stigebrandt, A., 2001. Chapter 2: physical oceanography of the Baltic Sea. In: Wulff, F., Rahm, L., Larsson, P. (Eds.), A System Analysis of the Baltic Sea, Pp. 19–74. Springer Verlag.
- Stramski, D., Boss, E., Bogucki, D., Voss, K.J., 2004. The role of seawater constituents in light backscattering in the ocean. Prog. Oceanogr. 61 (1), 27–56.
- Strickland, J.H.D., Parsons, T.R., 1972. A practical hand-book of sea-water analysis. Bulletin Journal of the Fisheries Research Board of Canada 167, 185–203.
- Suursaar, Ü., Kullas, T., Otsmann, M., 2001. The influence of currents and waves on ecological conditions of the Väinameri. Proc. Est. Acad. Sci. Biol. Ecol. 50, 231–247.
- Toming, K., Kutser, T., Laas, A., Sepp, M., Paavel, B., Nöges, T., 2016. First experiences in mapping lake water quality parameters with Sentinel-2 MSI imagery. Remote Sens. 8 (8), 640.
- Vaičiūtė, D., Bresciani, M., Bučas, M., 2012. Validation of MERIS bio-optical products with in situ data in the turbid Lithuanian Baltic Sea coastal waters. J. Appl. Remote. Sens. 6 (1), 1–20. <https://doi.org/10.1117/1.JRS.6.063568>.
- Vaičiūtė, D., Bresciani, M., Bartoli, M., Giardino, C., Bučas, M., 2015. Spatial and temporal distribution of coloured dissolved organic matter in a hypertrophic freshwater lagoon. J. Limnol. 74 (3).
- Veneranta, L., Urho, L., Lappalainen, A., Kallasvuo, M., 2011. Turbidity characterizes the reproduction areas of pikeperch (*Sander lucioperca* (L.)) in the northern Baltic Sea. Estuar. Coast. Shelf Sci. 95 (1), 199–206.
- Viehberg, F.A., Frenzel, P., Hoffmann, G., 2008. Succession of late Pleistocene and Holocene ostracode assemblages in a transgressive environment: a study at a coastal locality of the southern Baltic Sea (Germany). Palaeogeogr. Palaeoclimatol. Palaeoecol. 264 (3–4), 318–329.
- Vinterhav, C., 2008. Remote Sensing of Baltic Coastal Waters Using MERIS — A Comparison of Three Case-2 Water Processors. Master project (examensarbete, 30 ECTS). INK, Stockholm University.
- Wasmund, N., Nausch, G., Matthäus, W., 1998. Phytoplankton spring blooms in the southern Baltic Sea—spatio-temporal development and long-term trends. J. Plankton Res. 20 (6), 1099–1117.
- Werdell, P., Bailey, S., 2005. An improved in-situ bio-optical data set for ocean color algorithm development and satellite data product validation. Remote Sens. Environ. 98, 122–140.
- Woźniak, S.B., Meler, J., Lednicka, B., Zdun, A., Stoń-Egiert, J., 2011. Inherent optical properties of suspended particulate matter in the southern Baltic Sea. Oceanologia 53 (3), 691–729.
- Zaneveld, J.R.V., Roach, D.M., Pak, H., 1974. The determination of the index of refraction distribution of oceanic particulates. J. Geophys. Res. 79 (27), 4091–4095.
- Zibordi, G., Ruddick, K., Ansko, I., Moore, G., Kratzer, S., Icely, J., Reinart, A., 2012. In situ determination of the remote sensing reflectance: an inter-comparison. Ocean Sci. 8 (4), 567–586.